AD_____

Award Number: W81XWH-07-1-0474

TITLE: Replicating Physiological Patterns of Activity with Prosthetic Stimulation

PRINCIPAL INVESTIGATOR: Shelley Fried, Ph.D.

CONTRACTING ORGANIZATION: Boston VA Research Institute (BVARI)
Boston, MA 02130

REPORT DATE: July 2008

TYPE OF REPORT: Annual

PREPARED FOR: U.S. Army Medical Research and Materiel Command
Fort Detrick, Maryland 21702-5012

REPORT DOCUMENTATION PAGE

Form Approved
OMB No. 0704-0188

1. REPORT DATE *(DD-MM-YYYY)*	**2. REPORT TYPE**	**3. DATES COVERED** *(From - To)*
01-07-2008	Annual	11 JUN 2007 - 10 JUN 2008

4. TITLE AND SUBTITLE

Replicating Physiological Patterns of Activity with Prosthetic Stimulation

5a. CONTRACT NUMBER

5b. GRANT NUMBER
W81XWH-07-1-0474

5c. PROGRAM ELEMENT NUMBER

6. AUTHOR(S)
Shelley Fried, Ph.D.

E-Mail: shelleyfried@yahoo.com

5d. PROJECT NUMBER

5e. TASK NUMBER

5f. WORK UNIT NUMBER

7. PERFORMING ORGANIZATION NAME(S) AND ADDRESS(ES)

Boston VA Research Institute (BVARI)
Boston, MA 02130

8. PERFORMING ORGANIZATION REPORT NUMBER

9. SPONSORING / MONITORING AGENCY NAME(S) AND ADDRESS(ES)
U.S. Army Medical Research and Materiel Command
Fort Detrick, Maryland 21702-5012

10. SPONSOR/MONITOR'S ACRONYM(S)

11. SPONSOR/MONITOR'S REPORT NUMBER(S)

12. DISTRIBUTION / AVAILABILITY STATEMENT
Approved for Public Release; Distribution Unlimited

13. SUPPLEMENTARY NOTES

14. ABSTRACT
We want to develop more effective methods of neural stimulation in order to improve the clinical outcomes associated with retinal prosthetics. To accomplish this, we are investigating the mechanism(s) by which different types of retinal neurons respond to electric stimulation. Previous studies have shown that ganglion cells, the output cells of the retina, can be activated directly and exclusively with short duration stimulus pulses [1; 12; 24; 42]. However, the site of spike initiation in ganglion cells (e.g. the element with the lowest threshold) is not known. Here, we found that the lowest thresholds occurred along the proximal axon, about 40 <m from the soma; this region of low threshold was spatially coextensive with a band of dense sodium channels also centered about 40 <m from the soma. The sodium channel bands formed a homogeneous population for a given type of ganglion cell (e.g. alpha), but the properties of the band were different across different types (e.g. the lengths and locations varied). As expected from the differences in band properties, the size and location of the low threshold regions were also different for different ganglion cell types. We also showed that axonal thresholds can be quite low – in some cases, lower than those found in the proximal axon region. This raises the possibility that a small stimulating electrode can elicit widespread neural activity. We continue to explore the mechanism underlying axonal activation with the hope of learning how to limit activation to the region around the soma/proximal axon.

15. SUBJECT TERMS
Retinal prosthetic, retinal ganglion cell, electric stimulation, initial segment

16. SECURITY CLASSIFICATION OF:			**17. LIMITATION OF ABSTRACT**	**18. NUMBER OF PAGES**	**19a. NAME OF RESPONSIBLE PERSON**
a. REPORT	**b. ABSTRACT**	**c. THIS PAGE**			USAMRMC
U	U	U	UU	71	**19b. TELEPHONE NUMBER** *(include area code)*

Table of Contents

Introduction

The overall goal of this project's research is to develop more effective methods of neural stimulation in order to improve the clinical outcomes[20; 21; 37; 38; 50] associated with retinal prosthetics. To accomplish this, we are investigating the mechanism(s) by which different types of retinal neurons respond to electric stimulation. Previous studies have shown that ganglion cells, the output cells of the retina, can be activated directly and exclusively with short duration stimulus pulses[1; 12; 24; 42]. However, the site of spike initiation in ganglion cells (e.g. the element with the lowest threshold) is not known. The site of spike initiation is thought to influence the quality of the elicited percept since activation of ganglion cell axons results in spatially diffuse activity that presumably yields spatially diffuse percepts. Identification of the spike initiation site is also important because it provides insight as to the underlying mechanism of activation; this may help reduce the high threshold levels currently required to elicit percepts during clinical trials [19; 20; 38; 50]. We also want to understand whether the site of activation is consistent across different types of ganglion cell [8; 31; 39]. Knowledge of the variations that arise in activating different neural types may lead to stimulation methods that generate more physiological patterns of neural activity (and presumably a higher quality of elicited vision). Here, we propose to use a combination of physiology, anatomy and immunochemistry to identify the site of spike initiation in ganglion cells. Correlation of the physiological regions of low threshold to specific anatomical features will unambiguously identify the site of low threshold. An analysis of how differences in the spike initiation site modulate differences in the response to electric stimulation will yield insights as to the underlying mechanism(s) of spike initiation. In this report, we describe our progress during the first year of the grant. We have identified the site of spike initiation and found differences in the size and location of the site for different ganglion cell types. We have also included a manuscript that describes our findings (Appendix I); the manuscript is scheduled for submission in August 2008.

Body

Task 1

Determine activation threshold as a function of electrode position in each type of retinal ganglion cell.
(Months 1-18)

Goals as listed in the approved statement of work:

- Measure spatial profiles (threshold as a function of distance between stimulating electrode and soma) in each ganglion cell sub-type (Mos. 4-18).
- Measure threshold for electric stimulation at the soma in each ganglion cell sub-type (Mos. 1-12).

The objective of the first goal was to determine whether 'hotspots' of low threshold existed in retinal ganglion cells, e.g. what position of the stimulating electrode results in the lowest activation threshold. Previous computational[16; 41] and physiological studies[23; 43] each found different sites, however, all were in or around the soma/proximal axon region. The specific anatomical features postulated to be the source of the low thresholds included the soma, axon hillock, initial segment, axon bend and the thin section - the actual site of lowest threshold had remained unknown. For this goal, we are precisely mapping threshold as a function of the position of the stimulating electrode. This allows us to correlate the low threshold regions to specific anatomical features that we are identifying as part of Tasks 3 & 4.

Previous computational studies[16; 41] also suggest that positioning the stimulating electrode over the distal axon results in thresholds that are only slightly higher than those of the soma/proximal axon region. An understanding of axonal thresholds is important since activation of distal axons is likely to result in large, spatially diffuse neural activity [16; 41]. Work from Jensen et al[23] supports the notion of relatively low axonal thresholds, however their findings were restricted to a single type of ganglion cell (see below) and their methods did not allow precise correlation of physiology with anatomy. Therefore, we propose to measure thresholds along more distal sections of the axon and then correlate regions of low threshold to specific anatomical features (see Tasks 3 and 4).

The objective of the second goal in this task is to characterize the response differences between different ganglion cell types. It is well established that there are 12-15 different types of retinal ganglion cells in all mammalian species [39; 40; 47], including primate [8]; different types have different anatomical and physiological properties. Preliminary experiments suggested that both the absolute threshold levels as well as the spatial profiles of threshold are each different in different ganglion cell types. Correlating the response differences from different ganglion cell types to differences in the anatomical site that generates the responses (Task 4) will help to identify the mechanism by which the different responses arise. This analysis will also allow us to determine whether multiple features are correlated with low threshold. For

example, even though a low threshold hotspot might be at the axon hillock, we want to understand whether soma size (for example) also correlates with threshold. Finally, a thorough understanding of the response differences may ultimately be needed in order to develop stimulation paradigms that create patterns of neural activity that more closely resemble normal physiological patterns.

Spatial profile of threshold

A typical threshold 'map' for a directionally selective (DS) ganglion cell is shown in Figure 1 (left). The specific details of our methodology are provided in Appendix I (see Methods). As the map indicates, the region of lowest threshold (dark blue) is offset from the soma (circle): on average, the center of the low threshold region is approximately 40 µm from the edge of the soma for DS cells. We were able to orient the optic disk to the left during experimental setup (left/right refers to the orientation used in Figure 1). Therefore, since ganglion cell axons course towards the optic disk, the region of low threshold is likely to be on the proximal portion of the axon. Identification of the anatomical feature that is correlated with the region of low threshold was performed and is discussed in Tasks 3 and 4 as well as in Appendix I.

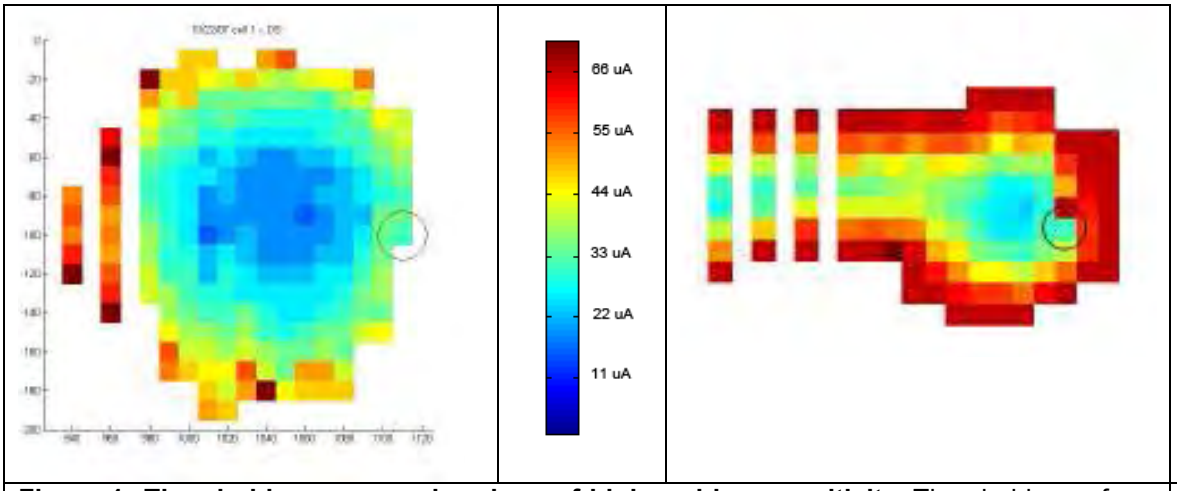

Figure 1: Threshold maps reveal regions of high and low sensitivity. Threshold map for a DS ganglion cell (left) and local edge detector (right). Each square represents a separate threshold measurement for that location of the stimulating electrode; 10 µm center to center spacing between adjacent pixels. The color of each pixel represents the threshold when the stimulating electrode was at that location. The colorbar (middle panel) applies to both maps. The circle indicates the approximate location of the soma. The height of the stimulating electrode was fixed at 25 µm above the retinal surface.Axes distances are in µm.

Repeating these measurements in six additional DS cells (data not shown) confirmed that the maps were consistent. Common features of all threshold maps include:

- A single region of low threshold in the soma/proximal axon region.
- The lowest level of threshold was consistent, ranging from 8-14 µA.
- Threshold increased monotonically in all directions from the center of the low threshold region.

- The center of the low threshold region was offset from the soma; the offset was always oriented towards the optic disk suggesting that the low thresholds arise from a portion of the proximal axon.

The consistency of these maps suggests that the underlying response mechanisms are similar in all DS ganglion cells. We are now investigating whether response mechanisms are similar in other ganglion cell types as well (see below).

Threshold maps from other ganglion cell types

Initially, we planned to use somatic thresholds (stimulating electrode positioned directly over the soma) as the basis for comparing thresholds between types. However, the maps from DS cells revealed that the lowest thresholds occurred when the stimulating electrode was offset from the soma and therefore we did not feel that somatic threshold was the appropriate parameter with which to perform comparisons. Since these maps provide a comprehensive overview of the spatial profile of threshold, however they allow not only a comparison of somatic thresholds between types but also allow a comparison of the size, location and absolute value of the minimum threshold region as well. Therefore, we remain focused on obtaining these maps for all ganglion cell types - not just measuring somatic threshold.

Threshold maps for other ganglion cell types are qualitatively similar to those of DS cells; a map from the local edge detector (LED) map is shown in Figure 1 (right panel). Comparison of the two maps reveals that both contain a single region of low threshold with threshold increasing as the stimulating electrode moves out in any direction from the center. However, in the LED type, the location of the low threshold region is much closer to the soma. Also, the size of the low threshold region is smaller for LEDs. These differences raise the possibility that the anatomical source of low thresholds is different in the DS and LED types – and possibly in other ganglion cell types as well. Our results to date suggest that this is in fact the case (discussed in Tasks 3 and 4).

We continue to record threshold maps for all ganglion cell types. However, identifying ganglion cell types unambiguously has proven more challenging than we originally anticipated. This is partly because both the physiological responses[9; 40] and anatomical features[39] used to sort cells can be very similar between certain types. As a result, we are focusing first on the types that are more easily categorized and we continue to work on methods for identifying the remaining types. We expect this task to be completed on schedule (Month 18).

Axonal thresholds

In addition to the threshold maps obtained in and around the somatic region, we also measured threshold maps along more distal portions of the axon (Fig. 2). As discussed previously, threshold decreased as the stimulating electrode was moved across the soma and then into the proximal axon. However, further movement along the axon, for distances up to 100 μm, resulted in increasing thresholds. Then, as the stimulating electrode moved even further along the distal axon, thresholds began to

decrease steadily and eventually reached a plateau. There was some variability in the both the slope of threshold decrease as well as the location and threshold level of the plateau. For example, in some cells, threshold reached a minimum when the stimulating electrode was only 400 µm from the soma. In other cases, the minimum threshold level found along the distal axon was slightly higher than that found in the proximal axon.

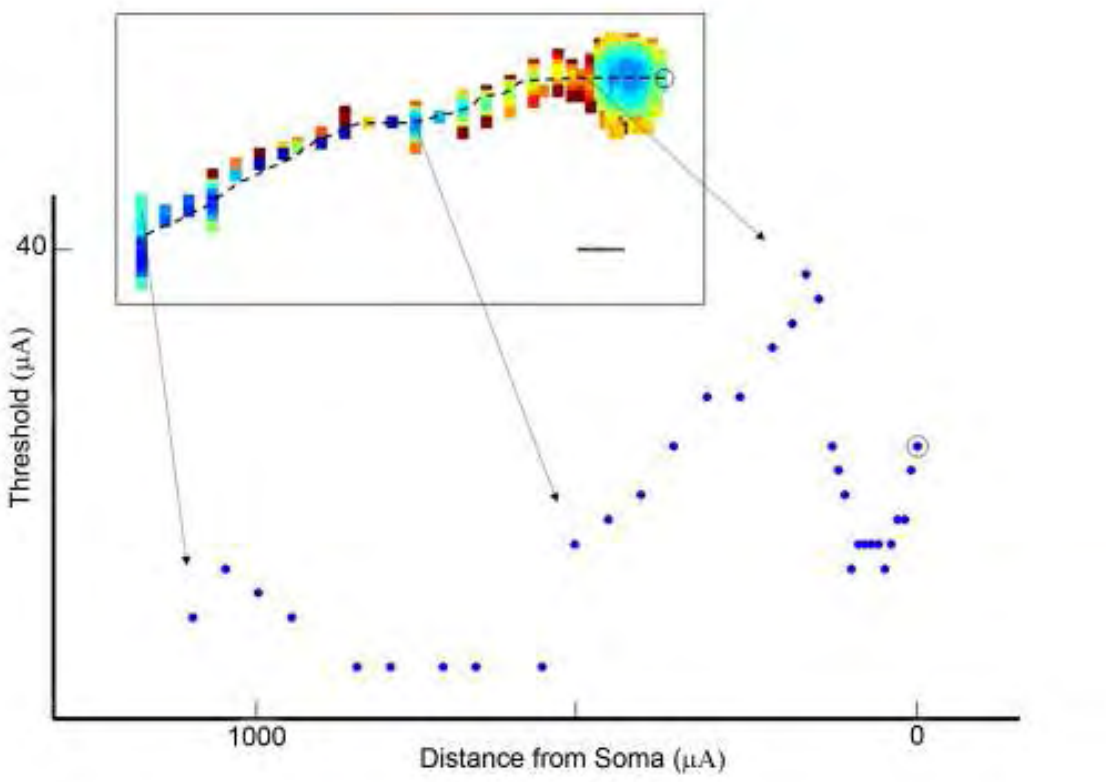

Figure 2: Low thresholds are found in segments of the distal axon. The inset shows a threshold map that extends out along the distal axon, approximately 1.1 mm from the soma. The gaps arise from incomplete sampling along the distal axon. Similar to Figure 1, each pixel of the threshold map contains an individual threshold measurement; the scale makes it difficult to resolve individual pixels. The colormap is identical to the one from Fig. 1. Threshold at each location along the axon (dashed line) is plotted as a function of distance from the soma. The circled point indicates the threshold level when the electrode was over the soma. Scale bar inset, 100 µm.

The descending-ascending-descending pattern of threshold in the proximal axon was somewhat surprising as it was not predicted by the computational models [16; 41]. We are currently exploring the sources of each component; our data so far suggests that different anatomical features contribute to the different components (discussed further in Tasks 3 & 4).

Summary: Task 1

- We have developed the methodology for measuring spatial profiles (Goal #1) and have completed maps for several ganglion cell sub-types (Figures 1 & 2).

- We will complete the maps for the remaining sub-types during the upcoming year.
- We have measured somatic threshold in several ganglion cell sub-types (Goal #2). However, as discussed in the body of this task, we no longer believe that somatic threshold is the ideal parameter with which to compare thresholds between types. Instead, measurement of lowest threshold (along the primary axon) is what we will use for comparison. This data will be captured (in addition to the somatic threshold) as part of the threshold map. This goal will be completed during the upcoming year.

Task 2

Determine the temporal response properties for each ganglion cell sub-type. (Months 10-21, erroneously listed as 4-14 on approved SOW)

Goals as listed in the approved statement of work:

- Determine the maximum rate for which one spike per pulse is elicited in each ganglion cell sub-type. Months 10-21
- Determine the response to high frequency stimulation (>250 Hz.) in each ganglion cell sub-type. Months 10-21

The low threshold regions identified within the threshold maps raised the question as to their underlying anatomical source. It seemed prudent to try to determine the source, as this knowledge would help to clarify all subsequent measurements as well as the comparisons between types. This required us to accelerate Task 3 which was originally scheduled from months 9-18 to a much earlier start (month 2). As a result, we spent a good deal of time this year on both Tasks 3 and 4 – Task 3 was originally not scheduled to begin until Month 9 of this year and Task 4 was not scheduled to begin until this upcoming year. The added effort for these two tasks came at the expense of a slight delay in starting the temporal studies associated with Task 2 which we are just now beginning. We anticipate having the temporal response properties completed during the upcoming year.

Summary: Task 2

- We have not yet begun to measure the temporal response properties – either for Goal 1 or Goal 2 of this task. As stated in the body of this task, and in Tasks 3 & 4, this comes as the result of accelerating some of the goals of Tasks 3 & 4.
- We plan to capture the temporal response properties (Goals 1 & 2) during this upcoming year.

Task 3

Measure the distribution of VGNaCs in each ganglion cell sub-type.
(Months 1 -27, erroneously listed as 9-18 in approved SOW)

Goals as listed in the approved statement of work:

- Measure the distribution of voltage-gated sodium channels in each ganglion cell sub-type using immunochemistry. Months 1-24.
- Determine which sub-types generate action potentials in their dendrites (evaluates functional viability of localized voltage-gated sodium channels). Months 19-27.

The overall objective of this task was to measure the distribution of voltage-gated sodium channels in each ganglion cell type. One of our original hypotheses was that regions of low threshold would be correlated with anatomical sections of the cell that contained high levels of sodium channels. Many other possible sources for the low thresholds (e.g. the soma and axon bend) were quickly eliminated (see Task 4), increasing the likelihood that our original hypothesis was valid.

For Goal 1, we used immunochemical methods to determine the distribution of voltage gated sodium channels in ganglion cells. A complete description of our methodology can be found in Appendix I (Methods). Briefly, we are localizing sodium channels using either Pan Sodium Antibody (PAN), an antibody that recognizes all isoforms of neuronal sodium channels[34], or by using antibodies for Ankyrin G, a structural protein associated with high density regions of voltage-gated sodium channels and typically found in the initial segment and nodes of Ranvier[4; 22; 26]. Our techniques are similar to those of previous groups that have explored sodium channels in retinal neurons [4; 45; 49]; these efforts have been greatly assisted by our collaborator Richard Masland, along with Tatjana Jakobs, Amane Koizumi and Bin Lin, post-doctoral fellows in his laboratory.

The objective of Goal 2 is to use physiological methods as a higher sensitivity detector of dendritic sodium channels. Several physiological studies indicate that retinal ganglion cells generate action potentials in their dendrites[32; 46], strongly suggesting the presence of voltage-gated sodium channels in the dendrites. Following the methods from one of these studies[32], we are able to similarly detect dendritic action potentials in DS ganglion cells (data not shown) even though we could not immunochemically detect the channels. The presence of sodium channels in the dendrites raises the possibility that they can be activated with electric stimulation[16] and therefore, our plan is to determine whether these channels can be activated effectively. Our threshold map data in DS cells suggests that dendritic sodium channels are not very sensitive to electric stimulation, however, it is not clear whether different stimulation paradigms might be more effective. We plan to perform this testing during the upcoming year.

Sodium channel distribution in DS ganglion cells

The pattern of PAN staining for a typical DS ganglion cell is shown in Figure 3 (left). The general appearance of a dense band of staining in the proximal axon is consistent with previous findings in both retinal[4; 45; 49] and non-retinal neurons. To determine the consistency of the sodium channel band within a single type of ganglion cell, we examined the PAN and/or Ankyrin G staining in 18 additional DS cells (Figs. 3, right). Although there was some variability in both the length and location of the sodium channel band across DS cells (Fig. 3, right), the population appears to be homogeneous. The mean length of the band was 28.69 +/- 4.65 µm; the mean location was 24.53 +/- 8.45 µm from the soma (near edge of the band to near edge of the soma). Interestingly, the mean location of the band center (38.87 µm) was coextensive with the mean location of the center of the low threshold region (39.79 µm) suggesting that the sodium channel band is the source of low thresholds. This is discussed further in Task 4. We were not able to find a correlation between sodium channel band length (or distance) and any other anatomical property of the cell (e.g. dendritic field diameter, dendritic area, soma size, etc.).

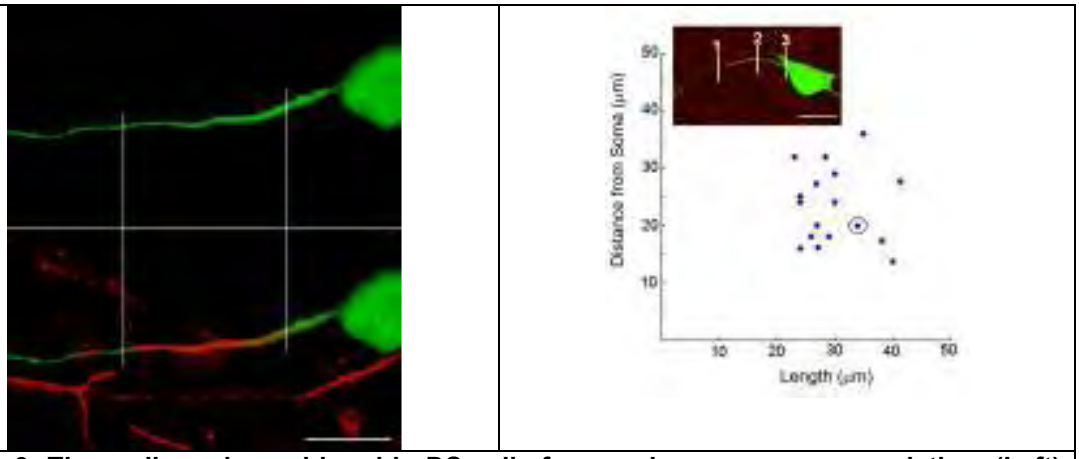

Figure 3: The sodium channel band in DS cells forms a homogeneous population. (Left) The dense sodium-channel region is co-localized to the region where the axon diameter decreases. *Top*: The soma and axon of a DS cell (green) that has been filled with a fluorescent dye. *Bottom*: The same DS cell (green) after immunostaining for PAN (red). One of the long immunostained bands (red) is coextensive with the DS axon. The other bands (red) are presumably associated with other (unfilled) ganglion cells. The vertical lines indicate the approximate extent of the dense sodium-channel region. Extension of the vertical lines up to the top panel reveal that the dense sodium-channel region is in a portion of the axon where the diameter transitions from large to small (compare the axon diameter at the right and left lines). Scale bar: 20 µm. **(Right):** Length and location analysis of high-density sodium-channel regions in DS cells suggests a homogeneous population. The length of the region (inset, distance between 1 and 2) was plotted vs. the distance between the soma and the proximal edge of the region (inset, distance between 2 and 3). Each point is from a different cell. The circled point is from the cell shown in the inset. Inset scale bar: 25 µm.

The region of dense staining is consistently (n = 16/18) found along the portion of the proximal axon in which the diameter tapers from the relatively large axon hillock section to the relatively narrow thin section that was originally described by Carras et al[6]. (Compare the axon diameter at the start and end of the sodium channel band in Fig. 3, left – top panel). This finding is consistent with the observation of Van Wart et al [45]. The region of dense staining commonly extended beyond the tapered region

into the thin section (n = 9/18). Less commonly, it extended into both the thick and thin sections (n = 6/18). The sodium channel band rarely extended into the thick section only (n = 2/18).

Sodium channel distribution in other ganglion cell types

We are currently investigating sodium channel distribution in other types of ganglion cells. The properties for the alpha ganglion cell type (G11 in the classification scheme of Rockhill et al[39]) are shown in Figure 4. The alpha cell sodium channel bands were longer than those for DS cells (40.62 +/- 5.39 μm vs. 28.69 +/- 4.65 (mean +/- std dev), $p<0.0001$, unpaired t-test). There was no statistical difference however between the mean distances (alpha: 26.87 +/- 5.51; DS: 24.53 +/- 8.45 μm, $p =0.382$, unpaired t-test). The sodium channel band in alpha cells is similarly located in the tapered portion of the proximal axon (data not shown).

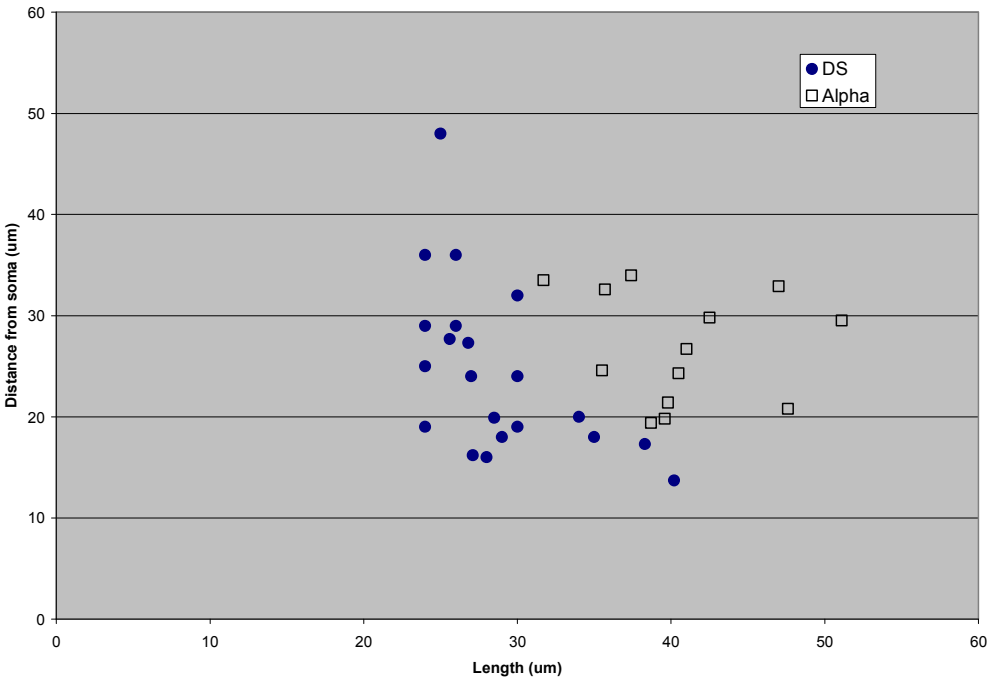

Figure 4: The sodium channel bands are different for different ganglion cell types. Similar to the data from Figure 3, each point represents the length and location of a measured sodium channel band. The location refers to the distance between the proximal edge of the band and the near edge of the soma. Dark, filled circles are from DS cells; unfilled squares are from alpha cells.

The reason(s) for the differences are not clear. Under normal conditions, the action potential is thought to be formed in the proximal portion of the ganglion cell axon (the initial segment), most likely within the dense band of sodium channels. It is tempting to speculate therefore that the differences in band properties contribute somehow to the different spiking responses observed in different ganglion cell types [31; 40]. Variations in band properties could modulate a wide range of properties related to the

spiking response, e.g. latency and/or spiking frequency. Differences in the band lengths corresponding to different ganglion cells have not been previously reported.

Summary: Task 3

- We have successfully developed the methods to analyze the voltage-gated sodium channel distributions in retinal ganglion cells (Goal #1).
- We have immunochemically measured the distribution of sodium channels in several different types; we plan to complete these measurements for remaining types in the next few months.
- We plan to begin localizing voltage-gated sodium channels using dendritic action potentials (Goal #2) during the second half of this upcoming year.

Task 4

Correlate dendritic field extent, soma size and distribution of VGNaCs with the activation threshold and dynamic range measurements described above. (Months 19-36)

Goals as listed in the approved statement of work:

- Correlate somatic threshold with dendritic field extent and distribution of voltage-gated sodium channels with the activation threshold and dynamic range measurements described above. Months 19-36.
- Correlate temporal response properties with dendritic field extent and soma size in each ganglion cell sub-type. Months 21-27.
- Correlate spatial profiles with voltage-gated sodium channel distribution in each ganglion cell sub-type. Months 28-33.
- Correlate spatial and temporal response properties with other morphologic features in each ganglion cell sub-type. Months 34-36.

The ultimate goal of this study is to learn where and how electric stimulation initiates spiking responses in retinal ganglion cells. To learn where the spike is initiated (Goal 3), we are correlating the threshold maps obtained in Task 1 to the sodium channel distributions obtained in Task 3. Originally, this task was not supposed to commence until the middle of Year 2 - after physiological results and immunochemical patterns had been obtained. However, the clear alignment between regions of low threshold and dense bands of sodium channels provided compelling reasons to begin sooner.

As part of Goal 4, we are correlating the spatial response maps of Task 1 to other anatomical features identified in Task 3 and also identified as part of this task (see below). Goals 1 and 2 of this task will begin during the upcoming year and continue through the final year of this grant.

Low thresholds do not arise from the soma or axon bend (Goal 4)

The region of low threshold in DS ganglion cells is offset from the soma. This finding is based on the threshold maps from six DS ganglion cells and is summarized in Figure 6 (left, blue lines). The average of all low threshold regions is centered ~40 μm from the edge of the soma. In addition, all bands are offset from the soma by at least 20 μm. Taken together, this suggests that the soma is not the source of low thresholds.

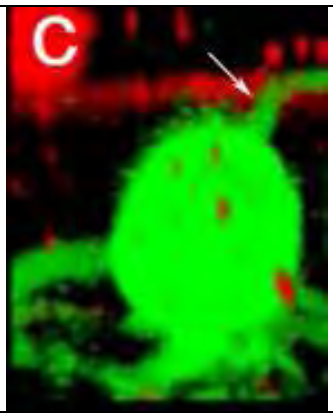

Figure 5: The axon bend occurs within 6 µm of the soma in DS cells. A DS ganglion cell soma (green) extends dendritic processes down into the inner plexiform layer and a single axon up to the nerve fiber layer (red). The axon emerges from the vitreal end of the soma (arrow) and ascends directly to the NFL. The bend occurs within the boundaries of the soma. Image width: 20 µm.

To study the alignment between the axon bend and the region of low thresholds, we obtained confocal image stacks of 18 DS ganglion cells. These images allowed us to view the three dimensional morphology, and therefore to determine the location of the axon bend. Figure 5 provides a typical cross sectional view of a DS ganglion cell soma as well as the emerging axon and bend (arrow). In 16/18 DS cells, we found that the bend occurred within 6 µm of the edge of the soma; in the cell of Figure 5, the bend actually occurs before the edge of the soma. The thin vertical line in Figure 6 (to the left of the thick 'SOMA' line) indicates a distance of 6 µm from the edge of the soma. Since nearly all axon bends occur between the two vertical lines, and therefore are offset from the low threshold region, it is likely that the bend is also not the source of low thresholds.

<u>The sodium channel band is the source of low thresholds in DS cells (Goal 3)</u>
Figure 6 (left) shows the alignment between the measured regions of low threshold (thin blue lines) and the measured sodium channel bands (thin red lines) for DS ganglion cells. The average low threshold region (thick blue line) and average sodium channel band (thick red line) were spatially coextensive. This suggests that the sodium channel band is the source of low thresholds. To provide further support, we were able to obtain a threshold map and then immunochemically stain the sodium channel band in the same cell (Fig. 6, right panels). The sodium channel band (between the two vertical lines, middle and bottom panels) is centered in the region of low threshold (dark blue pixels, top and middle panels), providing additional evidence that the band is the source of low thresholds.

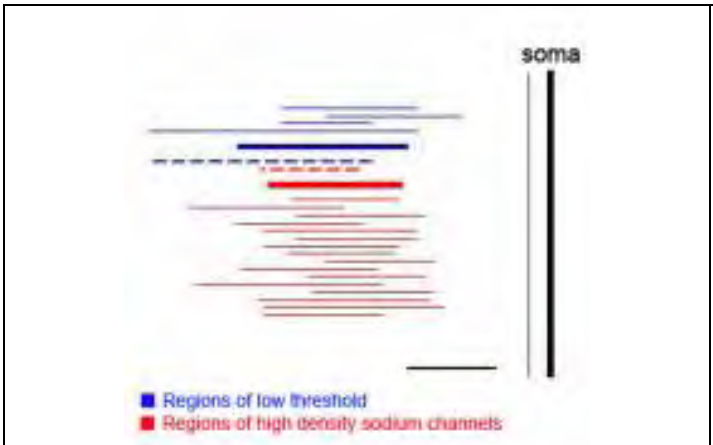

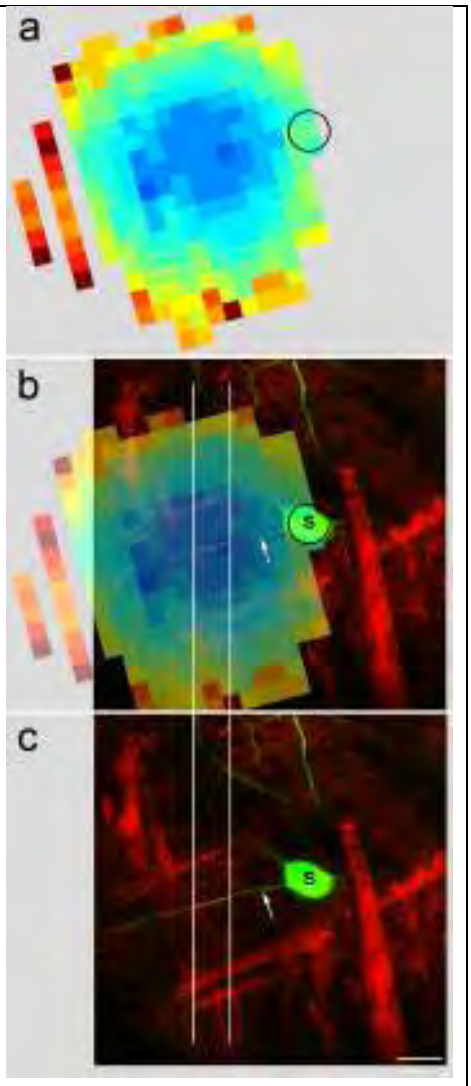

Figure 6: High density sodium-channel and low threshold regions are spatially co-extensive. (Left) The thick vertical line on the right indicates the edge of the soma. Each thin red line corresponds to a region of high density sodium channels: the length of the line is proportional to the length of the high-density region; the distance between the line and the 'soma' line is proportional to the distance between the high-density region and the soma. The thick red line represents the mean of all high-density regions. Similarly, each thin blue line corresponds to the length and position of each region of low threshold. The thick blue line represents the mean size and location of all regions of low threshold. The dotted red and blue lines correspond to the high-density region and low threshold region (respectively) from the one cell (right) in which both measurements were taken. The thin vertical line represents a distance of 6 μm from the soma; the region between the two lines is where most axon bends were found. Scale bar: 20 μm. **(Right)** (**a**) Threshold map of a DS ganglion cell. The map has been rotated ~20° in order to align it to the Ankyrin G image in (c) The threshold values given by each color are identical to those in Fig. 1. (**b**) Overlay of the threshold map with the Ankyrin G staining. The soma ('s') and axon (arrow) are clearly visible. The white vertical lines extend up from (c) and are used to clarify the region of high density Ankyrin G staining. (**c**) Ankyrin G staining in the same cell as (a). Scale bar in (c): 25 μm (applies to all panels).

<u>The source of low thresholds in other ganglion cells</u>

Our preliminary evidence suggests that the sodium channel band is approximately centered in other ganglion cell types as well (data not shown). We expect to complete this analysis for additional ganglion cell types later this year.

<u>Distal axon</u>

As described under Task 1, there is a second region of low thresholds located in the more distal axon. The exact location of this region is somewhat variable and as yet,

we have not been able to identify the underlying anatomical feature(s). We have observed that rabbit ganglion cell axons run as single fibers for several hundred microns before ultimately merging with a fiber band containing 10's or 100's of axon fibers. Our current hypothesis is that the low threshold plateau in the distal axon occurs as the single fiber joins the band. We are also exploring several different hypotheses to explain the threshold increase that occurs just distal to the low threshold region. We expect to better understand these phenomena within the next few months.

Summary: Task 4

- We have completed Goal 3 for DS cells (Fig. 6). We plan to complete this goal for the remaining types during the upcoming year.
- We plan to begin Goal 1 during the upcoming year.
- We plan to begin Goal 2 during the upcoming year.
- We have begun to look at several aspects of Goal 4 in DS cells (Figs. 5 & 6). We plan to continue this work with other types as we capture the maps (Task 1) and morphology. Additional summaries will become available during the upcoming year but the task will not be completed until Year 3.

Key Research Accomplishments

1. We have shown that threshold levels are lowest when the stimulating electrode is positioned over a portion of the proximal axon.

2. We have shown that the region of low threshold does not correspond to either the soma or the axon bend. Our results directly refute findings from two recent computational studies that each suggested that thresholds were lowest in one of these two regions.

3. We have shown that the region of low threshold corresponds to a dense band of sodium channels located within the proximal axon.

4. We have shown that the sodium channel band corresponds to a portion of the axon in which the diameter tapers from relatively large section associated with the axon hillock to the relatively thin section originally described by Carras et al.

5. We have shown that the sodium channel bands are consistent within a given type of ganglion cell but the bands vary from type to type. There is some overlap in band properties between different types. These difference may play a role in the different spiking responses (to light) generated in different ganglion cells. The differences are also likely to shape the response to electric stimulation and therefore different ganglion cell types may respond differently to electric stimulation.

6. We have shown that the threshold maps are also different across ganglion cell types; these differences presumably arise from the differences in the sodium channel bands.

7. We have shown that thresholds in the distal axon are somewhat variable and can be quite low – even lower than the levels found in the proximal axon. This finding contradicts findings from the two computational studies mentioned earlier (#2), as well as a physiological study, all of which suggest that the axonal thresholds are higher than those of the soma/proximal axon region.

8. We have prepared a manuscript detailing the above findings (Appendix I).

Reportable Outcomes

1. A manuscript detailing our identification of the source of low thresholds, the low axonal thresholds as well as the differences between ganglion cell types has been prepared for submission.

2. A total of six abstracts related to findings from this work have been accepted to date.

3. A total of six presentations related to this work have been made or have been accepted at upcoming conferences: Three at the most recent ARVO conference (April 2008), one at the Eye and the Chip conference (June 2008) and two will be presented at the upcoming BMES conference (September 2008). In addition, the PI has been invited to present this work at upcoming (2009) conferences in Bonn, Germany and Kyoto, Japan.

4. Our findings were included as part of a grant submitted by Nicolas Cottaris at Wayne State Medical School. One of our members (the PI) was listed as Co-Investigator on the Cottaris grant.

5. We have been awarded additional funding for additional capital equipment from the VA Healthcare System. This has allowed us to purchase a second patch clamp rig for use in these studies

6. We have begun a collaboration with Alyosha Molnar, Assistant Professor in Electrical Engineering and Computer Science at Cornell University, to develop a Hodgkin-Huxley type model in which to explore the responses of retinal ganglion cells to electric stimulation. We will also use the model to investigate the role of length variations in the sodium channel bands during normal retinal processing.

Conclusions

To improve the clinical outcomes associated with retinal prosthetics, we are investigating the response of retinal neurons to electric stimulation. Our findings provide direct answers to several open questions in this area and provide guidance for future studies. Our continuing efforts will lead to new, more effective methods of stimulation that reduce the high threshold levels currently associated with clinical trials. Our findings will also form the basis for methods that improve the quality of elicited percepts.

We have determined that the site of lowest threshold in retinal ganglion cells (the output cells of the retina) is a small portion of the proximal axon, ~40 μm from the soma. This region of low threshold is coextensive with a dense band of sodium channels also localized within the proximal axon. The identification of this site, presumably the site of spike initiation, answers a fundamental question relating to electric stimulation of retinal neurons; it also refutes predictions from two earlier computational simulations each of which predicted a different site (soma and axon bend).

Knowledge of the site of spike initiation also allows us to more effectively explore the mechanism(s) underlying activation. For example, we are investigating how individual properties of the electric field influence spike initiation; knowledge of the spike initiation site makes the investigation much more straightforward. Also, we can more clearly determine whether other neuronal elements (e.g. soma size) also contribute to threshold. These findings will contribute to a fundamental knowledge basis from which we can more rationally investigate the retinal response underlying clinical percepts. Ultimately, this knowledge basis will lead to improved methods of stimulation.

We found that the size and location of the sodium channel band was consistent within a given type of ganglion cell, however the band properties for each type were different. We are still studying the implications of this previously unreported finding; it is likely that the band differences influence the different spiking patterns generated normally by each type. There are several possible mechanisms by which this might occur however, and we are just beginning to investigate these different possibilities.

In addition to the role that the sodium channel bands play during normal light responses, band properties are also likely to influence the response to electric stimulation. We have found that the activation thresholds are different for different ganglion cell types; since our results here suggest that the sodium channel band is the source of the low thresholds, it seems reasonable to assume that differences in the band underlie the differences in threshold (e.g. long bands might result in low thresholds). As we gain insight into the response differences between different neural types, we will start to be able to predict the neural activity underlying clinical responses. Ultimately, this will help guide the design of new stimulation systems that

can selectively activate individual ganglion cell types. This will help elicit neural activity that more closely resembles the normal, physiological responses.

Finally, we found that axonal thresholds were quite low – in some cases they were lower than those found near the soma (in the proximal axon region). Low axonal thresholds result in a wider spread of neural activity and are therefore thought to enlarge the elicited percept. This has the effect of reducing spatial resolution and distorting the overall shape of the desired percept. Surprisingly, we found that axonal thresholds did not reach their lowest levels until the stimulating electrode was several hundred microns from the soma. As of the writing of this report, we have not yet identified the underlying anatomical or biophysical basis, however we have several different hypotheses that we are now exploring. We are investigating this mechanism, as one of the steps towards reducing the activation of axons (and thereby improving the quality of elicited percepts).

References

1 Ahuja, A. K., M. R. Behrend, J. J. Whalen, M. S. Humayun, and J. D. Weiland, 2008, The dependence of spectral impedance on disc microelectrode radius: IEEE Trans Biomed Eng, v. 55, p. 1457-60.

2 Boiko, T., A. Van Wart, J. H. Caldwell, S. R. Levinson, J. S. Trimmer, and G. Matthews, 2003, Functional specialization of the axon initial segment by isoform-specific sodium channel targeting: J Neurosci, v. 23, p. 2306-13.

3 Carras, P. L., P. A. Coleman, and R. F. Miller, 1992, Site of action potential initiation in amphibian retinal ganglion cells: J Neurophysiol, v. 67, p. 292-304.

4 Dacey, D. M., B. B. Peterson, F. R. Robinson, and P. D. Gamlin, 2003, Fireworks in the primate retina: in vitro photodynamics reveals diverse LGN-projecting ganglion cell types: Neuron, v. 37, p. 15-27.

5 DeVries, S. H., and D. A. Baylor, 1997, Mosaic arrangement of ganglion cell receptive fields in rabbit retina: Journal of Neurophysiology, v. 78, p. 2048-2060.

6 Fried, S. I., H. A. Hsueh, and F. Werblin, 2007, A method for generating precise temporal patterns of activity with prosthetic stimulation, *in* M. Humayun, J. Weiland, G. J. Chader, and E. Greenbaum, eds., Artificial Sight: Basic Research, Biomedical Engineering and Clinical Advances, Springer, p. 347-54.

7 Greenberg, R. J., T. J. Velte, M. S. Humayun, G. N. Scarlatis, and E. de Juan, Jr., 1999, A computational model of electrical stimulation of the retinal ganglion cell: IEEE Trans Biomed Eng, v. 46, p. 505-14.

8 Humayun, M. S., E. de Juan, Jr., G. Dagnelie, R. J. Greenberg, R. H. Propst, and D. H. Phillips, 1996, Visual perception elicited by electrical stimulation of retina in blind humans: Arch Ophthalmol, v. 114, p. 40-6.

9 Humayun, M. S., E. de Juan, Jr., J. D. Weiland, G. Dagnelie, S. Katona, R. Greenberg, and S. Suzuki, 1999, Pattern electrical stimulation of the human retina: Vision Res, v. 39, p. 2569-76.

10 Humayun, M. S., J. D. Weiland, G. Y. Fujii, R. Greenberg, R. Williamson, J. Little, B. Mech, V. Cimmarusti, G. Van Boemel, G. Dagnelie, and E. de Juan, 2003, Visual perception in a blind subject with a chronic microelectronic retinal prosthesis: Vision Res, v. 43, p. 2573-81.

11 Jenkins, S. M., and V. Bennett, 2001, Ankyrin-G coordinates assembly of the spectrin-based membrane skeleton, voltage-gated sodium channels, and L1 CAMs at Purkinje neuron initial segments: J Cell Biol, v. 155, p. 739-46.

12 Jensen, R. J., J. F. Rizzo, 3rd, O. R. Ziv, A. Grumet, and J. Wyatt, 2003, Thresholds for activation of rabbit retinal ganglion cells with an ultrafine, extracellular microelectrode: Invest Ophthalmol Vis Sci, v. 44, p. 3533-43.

13 Jensen, R. J., O. R. Ziv, and J. F. Rizzo, 2005, Responses of rabbit retinal ganglion cells to electrical stimulation with an epiretinal electrode: J Neural Eng, v. 2, p. S16-21.

14 Kordeli, E., S. Lambert, and V. Bennett, 1995, AnkyrinG. A new ankyrin gene with neural-specific isoforms localized at the axonal initial segment and node of Ranvier: J Biol Chem, v. 270, p. 2352-9.

15 O'Brien, B. J., T. Isayama, R. Richardson, and D. M. Berson, 2002, Intrinsic physiological properties of cat retinal ganglion cells: J Physiol, v. 538, p. 787-802.
16 Oesch, N., T. Euler, and W. R. Taylor, 2005, Direction-selective dendritic action potentials in rabbit retina: Neuron, v. 47, p. 739-50.
17 Rasband, M. N., E. Peles, J. S. Trimmer, S. R. Levinson, S. E. Lux, and P. Shrager, 1999, Dependence of nodal sodium channel clustering on paranodal axoglial contact in the developing CNS: J Neurosci, v. 19, p. 7516-28.
18 Rizzo, J. F., 3rd, J. Wyatt, J. Loewenstein, S. Kelly, and D. Shire, 2003, Methods and perceptual thresholds for short-term electrical stimulation of human retina with microelectrode arrays: Invest Ophthalmol Vis Sci, v. 44, p. 5355-61.
19 Rizzo, J. F., 3rd, J. Wyatt, J. Loewenstein, S. Kelly, and D. Shire, 2003, Perceptual efficacy of electrical stimulation of human retina with a microelectrode array during short-term surgical trials: Invest Ophthalmol Vis Sci, v. 44, p. 5362-9.
20 Rockhill, R. L., F. J. Daly, M. A. MacNeil, S. P. Brown, and R. H. Masland, 2002, The diversity of ganglion cells in a mammalian retina: J Neurosci, v. 22, p. 3831-43.
21 Roska, B., and F. Werblin, 2001, Vertical interactions across ten parallel, stacked representations in the mammalian retina: Nature, v. 410, p. 583-587.
22 Schiefer, M. A., and W. M. Grill, 2006, Sites of neuronal excitation by epiretinal electrical stimulation: IEEE Trans Neural Syst Rehabil Eng, v. 14, p. 5-13.
23 Sekirnjak, C., P. Hottowy, A. Sher, W. Dabrowski, A. M. Litke, and E. J. Chichilnisky, 2006, Electrical stimulation of mammalian retinal ganglion cells with multielectrode arrays: J Neurophysiol, v. 95, p. 3311-27.
24 Sekirnjak, C., P. Hottowy, A. Sher, W. Dabrowski, A. M. Litke, and E. J. Chichilnisky, 2008, High-resolution electrical stimulation of primate retina for epiretinal implant design: J Neurosci, v. 28, p. 4446-56.
25 Van Wart, A., J. S. Trimmer, and G. Matthews, 2007, Polarized distribution of ion channels within microdomains of the axon initial segment: J Comp Neurol, v. 500, p. 339-52.
26 Velte, T. J., and R. H. Masland, 1999, Action potentials in the dendrites of retinal ganglion cells: J Neurophysiol, v. 81, p. 1412-7.
27 Wassle, H., 2004, Parallel processing in the mammalian retina: Nat Rev Neurosci, v. 5, p. 747-57.
28 Wollner, D. A., and W. A. Catterall, 1986, Localization of sodium channels in axon hillocks and initial segments of retinal ganglion cells: Proc Natl Acad Sci U S A, v. 83, p. 8424-8.
29 Zrenner, E., D. Besch, K. U. Bartz-Schmidt, F. Gekeler, and V. P. Gabel, 2006, Subretinal chronic multielectrode arrays implanted in blind patients: Invest Ophthalmol Vis Sci, v. 47.

Appendix I

(manuscript draft)

Abstract

Electrically stimulating the retina of blind patients reliably elicits light percepts. However, their descriptions vary considerably and the mechanism by which they arise is not well understood. This lack of understanding may also contribute to the high thresholds needed to elicit phosphenes; clinical thresholds are typically several orders of magnitude higher than single cell thresholds in retinal explants. To better understand the mechanism by which retinal neurons respond to electric stimulation, we studied the site of spike initiation in retinal ganglion cells - previous computational and physiological studies suggested five different possibilities and the actual site remained unknown. To study this, we measured thresholds in a dense two-dimensional grid around each cell and found that a small section of the axon, about 40 μm from the soma, had the lowest threshold. Immunochemical staining revealed a dense band of voltage gated sodium channels in the same portion of the proximal axon suggesting that the sodium channel band is responsible for the low thresholds. We found additional regions of low threshold in the more distal axon, but the exact locations were variable and could not be correlated to specific anatomical and/or biophysical markers. Because axons traverse great distances across the retina, low thresholds in the distal axon present a considerable challenge to creating focal, predictable patterns of activation. In additional testing, we found quantitative differences between ganglion cell types: both the location of the proximal low

threshold region and the location (and size) of the corresponding dense sodium channel region were different.

INTRODUCTION

Several research groups are actively developing retinal prosthetics - devices designed to restore vision to blind patients by electrically stimulating surviving retinal neurons[7; 14; 18; 21; 37; 38]. The ability of this approach to elicit light percepts, called phosphenes, in blind patients has been successfully demonstrated although considerable variability in the size, shape, color and contrast of individual phosphenes has been reported. Although many factors are likely to contribute to the variability, a significant part is thought to arise from use of sub-optimal stimulation methods, e.g. methods that create non-physiological signaling patterns in retinal neurons. Lack of knowledge about appropriate stimulation methods may also underlie the high threshold levels required to elicit phosphenes; clinical threshold levels are typically several orders of magnitude larger than those required to elicit neural activity in animal studies (summarized in [42]).

The mechanism underlying the generation of phosphenes is not well understood. Short duration stimulus pulses activate ganglion cells (the output cells of the retina) [13; 15; 24; 42] however the extent of the region containing activated neurons depends on which part of the ganglion cell is activated: if a region at or near the soma has the lowest threshold, activation will be confined to neurons close to the stimulating electrode and the percept will presumably be focal. On the other hand, if axons, which traverse great distances across the innermost surface of the retina, are activated, the elicited percept will reflect the activity of ganglion cells both close to

and far from the stimulating electrode and the resulting percept will likely be diffuse and its appearance will be difficult to predict.

Previous studies report conflicting results as to which element(s) of the ganglion cell has the lowest threshold. Three different computer simulations each predicted different sites of lowest threshold: (1) the soma[16], (2) the characteristic bend in the axon[41] and (3) the distal edge of the initial segment[36]. A physiological study found the site of lowest threshold to be near the soma but, the anatomical correlate of the low threshold region was not identified [23]. Studies outside the retina consistently report the site of spike initiation to be on the axon, although both proximal (initial segment) [17; 35; 44] and distal portions[29; 30; 35] of the axon have been reported as having the lowest threshold. Ganglion cell axons are not myelinated but can still be activated by electric stimulation although the thresholds are higher than those for myelinated axons[27; 33; 48].

Taken together, previous studies suggest five possible regions as the site of spike initiation (lowest threshold) in retinal ganglion cells: (1) the soma, (2) the characteristic bend in the axon, (3) a region adjacent to the soma on the side distal to the optic disk, (4) the initial segment and (5) the unmyelinated axon. Recent studies have shown that the dendrites of some retinal ganglion cells initiate action potentials[32; 46] raising the possibility that some or all of the dendritic arbor may be sensitive to electric stimulation and therefore creates a sixth possibility. In this study

we use a combination of electrophysiology and immunochemistry to identify the site of minimum threshold in retinal ganglion cells.

METHODS

Animal preparation

The care and use of animals followed all federal and institutional guidelines, and all protocols were approved by the Institutional Animal Care and Use Committees of the Boston VA Healthcare System and/or the Subcommittee of Research Animal Care of the Massachusetts General Hospital. New Zealand white rabbits, ~2.5 kg, were anesthetized with injections of xylazine/ketamine and subsequently euthanized with an intracardial injection of pentobarbital sodium. Immediately after death, the eyes were removed.

ELECTROPHYSIOLOGY

Retina isolation

All procedures subsequent to eye removal were performed under dim red illumination. The front of the eye was removed, the vitreous was eliminated, and the eye cup was dissected so that the visual streak and regions ventral were left intact, all other areas were discarded. Three rectangular pieces, each ~5 x 7 mm, were extracted and stored in oxygenated Ames medium. Storage times ranged from 15 min to 6 h. Just before use, the retina was separated from the retinal pigment epithelium and mounted, photoreceptor side down, to a 10-mm square piece of Millipore filter paper (0.45 μm HA Membrane Filter) that was mounted with vacuum grease to the recording chamber (~1.0 ml volume). A 4-mm square hole in the center of the Millipore paper allowed light from below to be projected on to the photoreceptors.

Retinas were superfused continuously at 7-10 ml/min with Ames medium (Sigma; pH 7.4, 36°C), equilibrated with 95% O2-5% CO2.

Recording electrodes

Patch pipettes were used to make small holes in the inner limiting membrane, and ganglion cells with large somata were targeted under visual control. Spiking was recorded with a cell-attached patch electrode (5-6 MΩ), filled with superfusate. Whole cell patch-clamp electrodes (6-7 MΩ) were filled with (in mM) 112.5 CsMeSO4, 1 MgSO4, 0.0078 CaCl2, 0.5 BAPTA, 10 HEPES, 4 ATP-Na2, 0.5 GTPNa3, 5 lidocaine N-ethyl bromide (QX314-Br), and 7.5 neurobiotin chloride (pH 7.2). Alexa 488 (Molecular Probes) was added to the intracellular solution in order to visualize the dendritic morphology of recorded cells after the electrical recordings were completed. Two silver-chloride coated silver wires served as the ground and were positioned at opposite edges of the recording chamber each approximately 15 mm from the targeted cell.

Light stimulus and data acquisition

The stimulus presentation and data acquisition software was written by G. Spor, T. Muench and D. Balya. Light stimuli were projected on to the retina from below through an LCD projector (Dell) and focused onto the photoreceptor outer segments. Retinas were light adapted before the start of electrophysiological recordings. Light stimuli consisted of stationary flashed squares (size range: 100 - 1000 μm), 1-s duration, centered at the soma and moving bars (300x1800 μm moving at 600

μm/sec). Cells were classified as directionally selective (DS) if their response to the flashed 200 μm square was ON-OFF and if their response to back and forth motion of the bars was directional, e.g. spiking levels were considerably higher in one direction vs. the other[3]. Cells were classified as local edge detectors (LED) if their response to flashes of small light squares (≤200 μm) consisted of sustained spiking at both the onset and offset of the flash[40]. In these cells, the light response was greatly reduced for flashed squares of increasing size. Contrast levels were set to 200% unless specified. Data were analyzed in Matlab (MathWorks).

Electric stimulation / Construction of threshold maps

The use of cell-attached patch-clamp recordings allowed direct visualization of the elicited action potentials with no obfuscation from the stimulus artifact [13]. Previous studies[13; 24; 42] have shown that short duration stimulus pulses (~0.1 ms) directly activate ganglion cells and not presynaptic neurons eliminating confusion between pre- and post-synaptic activation. Electrical stimulation was delivered via a Platinum-Iridium electrode (MicroProbes). The impedance of the electrode was approximately 100 kΩ; the exposed area was conical with an approximate height of 35 μm and base diameter of 30 μm. Two silver-chloride coated silver wires served as the return; each was positioned at approximately 8 mm from the targeted cell and approximately 12 mm from each other.

At a given location of the stimulating electrode, a series of 10 biphasic pulses was delivered at 10 Hz; amplitude increased by 2 μA with each consecutive pulse. Each

biphasic pulse consisted of equal and opposite square waves (MultiChannel Systems hardware and software); cathodic pulses were delivered first and intervals between phases were typically 10 ms, which was large enough for the neural response to the cathodic pulse to be completed before the onset of the anodic phase. The lowest amplitude level at which 2 of 3 pulses (cathodic phase) elicited a spike was considered threshold (Fig. 1).

In most cases, the percentage of successful trials increased monotonically with increasing stimulus amplitude, allowing for a straightforward determination of threshold (Fig. 1b). In trials where threshold did not increase monotonically, determination of threshold was somewhat subjective (Fig. 1c). Therefore, we fit the raw data with a sigmoid curve (dotted lines, Figs. 1b, c) and defined threshold as the amplitude level at which the percentage of successful trials crossed 0.67 - or 2 of 3 pulses elicited spikes. For consistency the threshold level as determined with the sigmoid curve, was used for all data (monotonic and non-monotonic increasing).

After determining threshold at one spatial location, we moved the stimulating electrode to a new location and repeated the process. The position of the stimulating electrode was controlled with a precision micromanipulator (Sutter). The distance between adjacent measurements was typically 10 μm; the height of the stimulating electrode was fixed at 25 μm above the surface of the inner limiting membrane. This process allowed us to construct maps of threshold as a function of the position of the stimulating electrode.

[Figure 1]

IMMUNOCHEMISTRY

Retina isolation

The eyes were removed and immediately transferred to oxygenated Ames' medium (Sigma) for hemisection. The retinas were teased off the sclera using a fine brush.

Interphase/Perfusion chamber for the explant culture of adult rabbit retina

Pieces of rabbit retina of approximate 1 cm2 were placed ganglion cell side up on a 0.4 µm Millicell tissue culture insert (Millipore). The quality of the tissue after incubation depended on smooth attachment to the membrane. Filter stands (2 cm diameter, 1 cm high) were cut from the caps of 1 ml Monoject Tuberculin syringe jackets, so that the Millicell filter rested on four "stands" when it was placed into a 60×20 cell culture dish (Nunc). Approximately 25 ml Ames' medium (Sigma) containing 1% horse serum, 1% N2 supplement, and 100 U/ml penicillin, 100 U/ml streptomycin, 0.3 mg/ml L-glutamine (Invitrogen) were added to the dish, so that the retina was in contact with the medium via the Millicell filter over the photoreceptor side, and with the incubator atmosphere (5% CO2, 35°C, humidified) over the ganglion cell side. All further manipulations, including gene gunning, were carried out with the retina attached to the Millicell filter.

Gene transfer

Transformation of the plasmid pEGFP (GenBank accession number 6084; Clontech, Palo Alto, CA) into Escherichia coli (DH5) and bacterial cell culture was performed according to standard procedures (Sambrook et al., 1989). For large-scale preparations of purified plasmid, the Qiagen (Valencia, CA) Maxi Prep kit was used. The plasmid was delivered to cells in the ganglion cell layer via particle-mediated transfection[25; 28]. Gold particles were coated with the green fluorescent protein (GFP) plasmid according to the manufacturer's instructions. In brief, for each preparation, 12.5 µg of plasmid, 100 µl of 1 M CaCl, and 100 µl of 0.05 M spermidine stock solution were added to 12.5 mg of gold particles (1.6 µm; Bio-Rad, Hercules, CA) under continuous, slow vortex. Plasmid was allowed to attach to the gold particles for 10 min before recentrifugation and resuspension in absolute ethanol. The gold-plasmid suspension was then applied to the inner surface diameter of plastic tubing using a tube prep station (Bio-Rad) and dried in place with nitrogen. The gene gun (Bio-Rad) was loaded with the gold plasmid-coated tubing. A nylon mesh (R-CMN-90; Small Parts Inc., Miami Lakes, FL) was placed at the nozzle of the gun to obtain better gold particle dispersion. The gun was primed to 115 psi, and the retina was flattened out on the Millicell filter. The nozzle was placed over the entire retina and fired. The retina was immediately rinsed in the above fresh Ames medium and placed on a rocker inside an incubated chamber (30°C) for two days with daily medium changes. This time is sufficient to allow expression of GFP, leading to bright labeling of individual ganglion cells of various types, and other cells in the ganglion

cell layer (mainly displaced amacrine cells). A total of 18 well-labeled cells were chosen for imaging and analysis.

Immunohistochemistry reagents

All antibodies used have been previously characterized. Mouse monoclonal anti-ankyrin-G antibody described by Jenkins et al. (2001) was purchased (cat. no. 12719; Santa Cruz Biotechnology, Santa Cruz, CA). K58/35, mouse monoclonal pan-specific anti-Nav referred to as PAN, described in detail in Rasband et al. (1999) was purchased (cat. no. S8809; Sigma Aldrich, St. Louis, Mo). Rhodamine mouse IgG secondary antibodies were used for visualization of primary antibodies (Jackson Immunoresearch, West Grove, PA).

Immunostaining

After gene transfer and incubation for 2 days, the retinas were fixed with 4% paraformaldehyde for 25-30 minutes at room temperature(RT) and washed 3x5 minutes in PBS, then placed in blocking solution consisting of 4% Donkey Serum in PBST (PBS + 0.3% TritonX). Primary antibodies were diluted in blocking solution and applied to the tissue for three to four days at RT. They were then washed 3x5 minutes in PBS. Secondary antibodies were diluted in blocking solution and applied at RT in the dark for one day. After washing 3x5 in PBS, the retinas were mounted in Vectashield (Vector Laboratories, Bulingame, CA). In the one cell in which both threshold maps and immunochemical staining were obtained, we used Streptavidin with Alexa Fluor 488 conjugate 2mg/ml (Invitrogen Molecular Probes); tissue was

fixed for 30 minutes, PB 3x 5 minutes and then 0.5 µl placed in 500 µl blocking solution overnight.

Data acquisition and analysis

Individual cells were imaged using a confocal microscope (Radiance, BioRad) with water immersion objectives (25x/0.8 Plan Apochromat, 40x/1.2 C-Neofluar, or 63x/1.4 C-Neofluar, all from Carl Zeiss Microimaging). Through-focus series of images were taken of labeled cells in the ganglion cell layer. Optical sections were taken at a thickness of .25um and .5um. The resulting images were adjusted for brightness and contrast with volume reconstruction software (VolView2, Kitware). The images were median filtered and collapsed into a maximum intensity projection in ImageJ software(Bethsda, MD) and VolView. Figures show planar projections of a series of successive confocal images. Using ImageJ software, lines were drawn at the proximal and distal edges of the high density region - the length of the high density region was taken as the distance between the two lines. A third line was drawn at the edge of the soma where the axon emerges - the distance between the soma and the high density region was taken as the distance between this line and the line at the proximal edge of the high density region. Images were formatted in Photoshop CS2 (Adobe).

Alignment of threshold maps and immunochemical staining

To align the ‘map’ of threshold measurements with the immunochemical images from the one cell in which we were able to capture both, we aligned an approximately 1.1

mm section of the axon from the immunochemical plot to the ‘axonal’ region of the threshold map (see Figure 9 inset). The ‘twists and turns’ were similar in both plots and were used in conjunction with the known position of the soma in both plots to generate a precise alignment.

RESULTS

We measured the threshold to initiate action potentials as a function of stimulating electrode position in six directionally selective (DS) ganglion cells. In one of these cells, we also were able to immunochemically characterize the location of voltage gated sodium channels, allowing a direct comparison with the location of the low threshold region. To compare the location of the low threshold region to the high sodium channel region across the population, we characterized the distribution of sodium channels in 17 additional DS cells. We examined the three dimensional morphology of each of the 18 'immunochemistry' cells in order to compare the location of other features thought to play a role in threshold level (e.g. the axon bend) to the regions of low threshold. To determine whether there were differences across different types of ganglion cells, we characterized the high density sodium channel region in 54 additional non-DS ganglion cells and measured threshold maps (n=2) in one other type (the local edge detector, 'LED').

Threshold maps

We refer to the plot of threshold vs. position of the stimulating electrode as a threshold map. A typical map is shown in Figure 2a. The color of each square on the map represents the measured threshold at that spatial location. As an example, the colored squares representing the thresholds determined in Figures 1b and 1c are labeled ('b' and 'c' respectively).The location and approximate size of the soma is depicted by the black circle.

[Figure 2]

The region of minimum threshold is offset from the soma

The overall appearance of the threshold map suggests a central, circular region of low threshold surrounded by concentric rings of increasing threshold. This is more clearly seen when the same data are replotted as a contour map (Fig. 2b) in which a single color represents a larger range of threshold levels. In this view it is apparent that the lowest threshold levels (dark blue) are surrounded by rings of increasing threshold levels (e.g. light blue, yellow, red). This arrangement suggests a single region in which stimulation thresholds were relatively low with threshold increasing as the stimulating electrode is moved away. The region of lowest threshold was always offset from the soma (n=6/6).

After emerging from the soma, ganglion cell axons course towards the optic disc, where they exit the retina and become the optic nerve. During preparation of our slides, the optic disk was placed on the left side (left/right orientation is as seen in Figure 2) so that axons generally coursed to the left. With this arrangement, the region of low threshold was always offset to the *left* side of the soma (near where the axon emerges from the soma). This suggested that a portion of the axon close to the soma (bend, hillock, initial segment, etc.) might be the target of stimulation.

Imaging Na+ channel distribution

Electric stimulation is thought to initiate spiking through voltage gated sodium channels (see [35] for a review) suggesting that high density regions of such channels are likely to have the lowest thresholds. In the retina, sodium channels have been found in the soma[10; 11], dendrites[32; 46], initial segment[4; 45] and axons[10; 11]. In addition, high density sodium channels have been reported in the nodes of Ranvier along myelinated axons[26] however, the axons of retinal ganglion cells are not myelinated and therefore do not contain nodes of Ranvier.

Our general approach for visualizing sodium channel distribution is illustrated in Figure 3. Nearly all of the DS ganglion cells studied (17/18) were transfected with a plasmid containing green fluorescent protein (GFP); plasmids were attached to gold particles and delivered via genegun (see Methods). After two days incubation, GFP expression was evident in 10-20 brightly visible ganglion cells per retina. DS cells were identified by several characteristic morphological features[2; 39] including a large (~25 μm) soma, a bistratified dendritic tree as well as recursive dendritic processes (Fig. 3a).

The band of high density sodium channels was visualized by immunochemical processing for one of two antibodies associated with sodium channels of the axon: (1) Ankyrin G, a structural protein associated with high density sodium channels found at the initial segment[22] and at nodes of Ranvier[5] or (2) Pan Sodium Antibody (Pan) which binds to all voltage gated sodium channels in retinal ganglion cells[4; 45]. Once a cell was confirmed as DS, high magnification was used to

examine the proximal axon, approximately 150 μm length, as it emerged from the soma (Fig.3b). Overlay of the Ankyrin G staining and the filled ganglion cell (Fig. 3d) revealed that one of the long thin bands of dense Ankyrin G staining corresponded with a portion of the ganglion cell axon (region between vertical lines). It is likely that the other long thin bands in Figure 3c are associated with axons of other ganglion cells that were not filled with GFP and therefore not visible. We also observed punctate labeling in the ganglion cell layer that was highly variable across preparations and is likely a result of non-specific binding of the Ankyrin G antibodies. We did not investigate the source of this 'noise' since it did not interfere with subsequent analysis of the initial segment. Similar results were obtained when Pan was used (Fig. 3e-h). Pan allowed visualization of the axon (used in subsequent analysis) while Ankyrin G staining resulted in clearer images.

In one case we were able to obtain immunochemistry in a DS cell with which we had previously obtained threshold recordings (1 of the 6 cells described in Fig. 2). Here, we used a different method to image the dendrites: after completion of threshold measurements, a whole cell patch was established with neurobiotin inside the patch clamp electrode. The cell was subsequently labeled via a GFP-streptavidin conjugate which allowed imaging of the dendrites. Immunostaining for sodium channels was done using Ankyrin G as described above.

[Figure 3]

We quantified the physical properties of the region of high density staining in a total of 18 DS ganglion cells - 11 treated with Ankyrin G and 7 treated with Pan (Fig. 4). Using Ankyrin G, the mean length of the high density region was 27.8 ± 4.2 μm and the mean distance from the soma was 24.0 ± 6.3 μm. Using Pan, the mean length was 31.4 ± 6.1 μm and the mean distance from the soma was 20.4 ± 5.9 μm. There was no statistical difference between the length or distance-to-soma measures ($p = 0.167$ and 0.266, respectively, unpaired t-test) when values from Ankyrin G and Pan were compared.

[Figure 4]

The variability in length and location of the high density sodium channel region was somewhat surprising; originally we had expected these regions to be more tightly clustered. Closer analysis revealed that the region of high density staining was spatially aligned with the portion of the axon in which the diameter transitioned from the relatively large axon hillock to the relatively thin diameter approximately 40 μm from the soma (Fig. 5a). Although the length and location of the transition region was also variable, the high density sodium channel region consistently corresponded to the transition (n=16/18). In many cases the sodium channel region was longer than the taper and so it extended into thick and/or thin portions of the axon.

[Figure 5]

High density sodium channels are centered in low threshold region

Since the region of low threshold and the region of high sodium channel density were both localized to a portion of the axon in close proximity to the soma, we wanted to determine whether these two regions overlapped. To examine this we plotted each of the regions of high density sodium channels and each of the regions of low threshold in a single plot (Fig. 6). Each region of high density sodium channels was represented by a single line (red) such that the length and position of the line corresponds to the length and position of the region. The vertical line on the right is used to represent the soma. Each region of low threshold is similarly scaled and aligned (thin blue lines). We computed the mean region of low threshold and the mean region of high sodium channel density (thick blue and red lines respectively) - the close alignment of the two regions suggests the region of high density sodium channels as the source of low thresholds.

[Figure 6]

We were able to confirm the correspondence between the low threshold and high density sodium channel regions by making both measurements in a single cell (Fig. 7, n=1). The two procedures each required a different mounting of the retina; therefore it was necessary to align (see Methods) the threshold map (Fig. 7a) obtained in the first procedure to the Ankyrin G immunostain (Fig 7c) obtained in the second procedure. Overlay of the two plots (Fig. 7b) reveals that the region of high density sodium channels is approximately centered in the region of low threshold providing

further support for the high density region as the ‘target’ of electric stimulation. Lines representing the low threshold and high density sodium channel regions for this cell were added to the summary plot (Fig. 6, dashed red and blue lines respectively). While there is clear alignment between the two regions, the region of low threshold extends beyond the region of high sodium channel density; it is not clear why this is so (Discussion).

[Figure 7]

Is the axon bend aligned with the region of low threshold?

A recent computational study[41] suggests that the lowest activation threshold is found along the axon as it moves inward (towards the vitreous) and bends to run along the nerve fiber layer (NFL). However, that simulation assumed a uniform density of sodium channels along the axon; our earlier results (Fig. 3) suggest that sodium channel density is not uniform in this region and therefore it is difficult to compare their findings to our results. Nevertheless, we wanted to determine whether the region of low threshold and the axon bend region were spatially aligned. In 16/18 DS ganglion cells whose morphology we examined, the axon bend emerged from the vitreal half of the soma and within 5 μm curved to run along the NFL (Fig. 8a). In cases in which the axon did not immediately rise up to enter the NFL, we generally found that the axon was ‘trapped’ below a bundle of axons; the single emerging axon ran parallel for sometimes as much as 125 μm before finally curving up to enter the NFL (Figs. 8b, g)

In many of the DS ganglion cells we observed, the axon, after reaching the NFL, descended back down towards the ganglion cell layer before curving up and returning to the NFL (Fig. 8c). In a few cases, multiple downward/upward oscillations were present. Interestingly, these oscillations appear to be the result of 'collisions' with axon fiber bundles (Fig. 8d-f). Using a combination of cross-section, whole mount and oblique views, the axon from Figure 8c is seen to descend as it approaches a bundle of axons (BAF). The axon fiber curves around the bottom of the bundle and then re-ascends to run along the NFL. Most axon fibers often ran for at least several hundred microns before joining an axon bundle although we did not formally quantify the exact distance.

[Figure 8]

The consistency in the location of the axon bend - in 16/18 DS cells it occurred within 5 μm of the soma - suggests that the axon bend itself is not associated with the low threshold region. The dotted vertical line in Figure 6 represents a distance of 5 μm from the soma; axon bends typically occur between the two vertical lines. In the one cell in which we were able to obtain both the threshold map and Ankyrin G immunostaining, we were able to directly compare the region of low threshold to the axon morphology (Fig. 8g). The cross sectional view of the cell reveals that the axon extends horizontally for approximately 80 μm before bending up towards the NFL. The region of low threshold (blue bar) is located along the straight portion of the axon

(no bend) providing additional evidence that the axon bend is *not* within the low threshold region.

In this same cell, the point of lowest threshold occurs while the axon is still running horizontally within the ganglion cell layer; the distance between the axon and the electrode is relatively large in this region. Interestingly, threshold levels *increase* as the axon ascends towards the NFL (the distance between stimulating electrode and axon is *decreasing*). This is surprising since threshold levels are known to decrease with decreasing distance between target and electrode. This suggests that the density of sodium channels is a more important component of threshold level than the distance between electrode and axon, at least in this region. We had the general impression that sodium channel density was lower just beyond the high density region suggesting that the increase in threshold in this region may arise from a decrease in sodium channel density.

Threshold levels in the distal axon

We were able to measure threshold levels at intermittent locations along the distal axon (>200 μm from the soma) in three of the six DS cells in which threshold maps were obtained (Fig. 9). While there was variability in the overall pattern, we consistently found several sites along the distal axon that had low thresholds. In some cases, threshold levels were even lower than the levels associated with the region of high sodium channel density (compare threshold levels at ~650 μm from the soma to those at ~ 50 μm). Although antibodies for Pan revealed sodium channels

along the distal axon, it did not allow us to discern whether there were local regions of increased density. We were not able to determine the cause of the low threshold levels or determine the reason for the variability (Discussion).

[Figure 9]

Differences across ganglion cell types

There are approximately 12 different types of retinal ganglion cells[8; 9; 39; 40]; each detects different features of the visual world and uses a different pattern of spiking to transmit information to higher visual centers[9; 31; 40]. The underlying anatomy and biophysical properties are different for each type raising the possibility that the region of high density sodium channels and/or region of low threshold may also be different in different types. To investigate this, we measured threshold maps in two local edge detectors (LED) - one of the other ganglion cell types (Fig. 10a, left). Comparison between the LED map (left) and the DS map (right) is shown in Figure 10a. While the general shape of the maps is similar, the size of the low threshold region is considerably larger for DS cells. The difference in low threshold regions between LEDs and DS cells suggests that the dense sodium channel region is different as well.

We imaged the high density sodium channel regions in 54 non-DS cells and found considerable diversity across the population (Fig. 10b). For example, the length (compare Figs. 10b, left and middle panels) and distance to the soma (compare Figs. 10b, middle and right panels) of the dense sodium channel regions were highly

variable. In DS cells, the dense sodium channel region was never less than 20 μm from the soma (0/18) while in some non-DS cells the dense sodium channel region was adjacent to the soma. This suggests that the dense regions are different for different ganglion cell types and further suggests that the threshold maps may be different for each type as well. We also found variations in the axon bend morphology between ganglion cell types (Fig. 10c) although we did not systematically evaluate these differences.

[Figure 10]

DISCUSSION

The goals of this study were to learn which regions of the retinal ganglion cell are the most sensitive to electric stimulation and to determine the cellular structure(s) that underlie lower thresholds. Four previous studies in the retina each found that a different part of the neuron had the lowest activation threshold, while studies outside the retina suggested a fifth possibility. As a first step toward resolving this, we measured threshold in response to electric stimulation in a large number of locations around one specific type of ganglion cell, the DS cell. After identifying the regions that had the lowest threshold, we used a combination of morphological and immunochemical analyses to correlate the region(s) of low threshold to specific morphological features.

We found the lowest thresholds in two different portions of the DS ganglion cell. The first region was a small section of the proximal axon centered approximately 40 μm from the soma (Fig 2); the second region was also on the axon but its exact location was variable although typically several hundred microns from the soma (Fig. 9). This arrangement is supported by previous studies in non-retinal neurons that found either the initial segment or the axon were had the lowest threshold in response to electric stimulation[17; 29; 30; 35; 44].

The region of low threshold near the soma was closely aligned with a region of high density sodium channels also centered ~40 μm from the soma (Fig. 3), a correspondence (Figs. 6, 7) suggesting that the high density sodium channels may

be responsible for the low thresholds in this region. Although there was variability in both the size and location of the high density sodium channel region, it was typically positioned on the portion of the axon in which the diameter was decreasing (Fig. 5) - from the large diameter associated with the axon hillock to the small diameter section originally described by Carras et al[6]. The sodium channel region was often longer than the tapered region and extended into either the thick or thin part of the axon (or both).

Thresholds in the distal axon were comparable to the lowest threshold levels in the proximal axon and in some cases were even lower (Fig. 9). This was somewhat surprising, for several reasons. First, our immunochemical staining suggests that the density of sodium channels is highest in the proximal axon. This is supported by previous work in retinal ganglion cells[10; 11] and the ratio of densities in the proximal vs. distal axon suggested by our findings is even higher than earlier reports. Lowest thresholds are typically associated with high sodium channel densities. Second, we could not find a systematic difference in axon position along the distal axon; e.g. the axon was not significantly closer to the stimulating electrode in the distal axon. In fact, our results suggest that the axon may sometimes move further away from the stimulating electrode in portions of the distal axon (Fig. 8). Finally, ganglion cell axons are typically not myelinated and previous studies have shown that thresholds are higher in non-myelinated axons. The combination of higher density sodium channels, lack of myelination and approximately equal distances to

the stimulating electrode suggest that thresholds in the proximal axon should be lowest.

Previous studies report that axons of the rabbit retina are myelinated in a small region around the optic disk. Although the tissue used in our study was quite far from the optic disk, it is nevertheless possible that myelination extends further than previous reports indicate. Even if this is the case, it is not clear whether this would be sufficient to lower thresholds below those of the proximal axon. Further study is warranted to determine the anatomical or biophysical basis underlying low threshold levels in the distal axon.

Discrepancies in the activation site

It is likely that the differences in sodium channel density found in our study vs. those used in previous computer simulations are responsible for the differences in the identified sites of low threshold. Although we did not quantify the actual densities, the patterns of Ankyrin G and PAN staining found in our study (Fig. 3) suggest a dense band of sodium channels confined to a narrow portion of the proximal axon while the sodium channel concentration outside the region of dense staining is considerably lower. In contrast, the previous computer simulations used sodium channel concentrations that were more uniform. We did not attempt to re-run those simulations but speculate that modifying the sodium channel concentrations to the levels suggested by this study would shift the predicted low threshold regions to agree with ours.

Implications for focal stimulation in clinical trials

Thresholds in portions of the distal axon were comparable to the lowest thresholds found in the proximal axon (the region of high density sodium channels)(Fig. 9). This suggests that a single stimulus applied to the retinal surface could activate both ganglion cells whose proximal axon is close to the electrode and ganglion cells whose distal axon passes close to the electrode. The resulting percept would presumably be 'diffuse' reflecting the wide spatial extent of activated.

This result seems in conflict with results from some clinical trials, in which percepts were reported as 'focal'. There are several possible explanations as to how both findings could be valid. For example, previous in vitro studies[13; 24; 42] found that long duration pulses (~1 ms) activate ganglion cells both directly (one spike per pulse) and indirectly, through activation of bipolar cells, generating a burst of spikes after each pulse. The net result for long pulses is two phases of spiking - a single spike that occurs within 1 ms of the onset of the pulse followed by a burst of spikes that occurs several milliseconds after completion of the stimulus pulse. While ganglion cell axons travel great distances, bipolar cell axons are quite short; it is likely therefore that bipolar cell activation is limited to the local region around the electrode. This suggests that the response to a long pulse may consist of a single spike in several diffuse ganglion cells followed by a burst of spikes in several neighboring ganglion cells. It is possible that the single spike is not 'visible' to the patient while the (focal) burst of spikes is.

Another possibility is that the axons that pass closest to the stimulating electrode are from neighboring regions of the retina. Activation of these cells leads to a percept that is larger than it would be if axon fibers were not activated. The 'larger' percept might still be considered 'focal' by the patient.

Differences across ganglion cell types

The physical dimensions of the region of high density sodium channels varied considerably across the population of non-DS ganglion cells (Fig. 10b). The variability across the entire population was larger than that of the single DS type suggesting that the properties of the dense sodium channel regions may be different for different types. It is tempting to speculate that these differences contribute to the differences in light responses found between types. The mechanism by which this occurs is not clear but perhaps the size and location of the high density region somehow modulate the threshold for spike initiation and/or the maximum spike frequency. The position of the high density sodium channel region relative to the axon taper may also play a role.

Threshold maps for LED ganglion cells were different than those from DS cells (Fig. 10a) supporting the above hypothesis that distributions of low threshold regions and corresponding high density sodium channel regions are different for each ganglion cell type. In addition, the smaller region of low threshold in the LED suggests that LED threshold levels are higher than DS cells perhaps because of differences in the

length and/or density of the sodium channel region. Our hope is that we may be able to use these differences between different types to develop methods for selective activation of individual ganglion cell types. This would eventually allow us to create more complex (physiological) patterns of stimulation with prosthetic electrodes and hopefully improve the quality of elicited percepts.

References

1 Ahuja, A. K., M. R. Behrend, J. J. Whalen, M. S. Humayun, and J. D. Weiland, 2008, The dependence of spectral impedance on disc microelectrode radius: IEEE Trans Biomed Eng, v. 55, p. 1457-60.

2 Amthor, F. R., E. S. Takahashi, and C. W. Oyster, 1989, Morphologies of rabbit retinal ganglion cells with complex receptive fields: J Comp Neurol, v. 280, p. 97-121.

3 Barlow, H. B., and W. R. Levick, 1965, Mechanism of Directionally Selective Units in Rabbits Retina: Journal of Physiology-London, v. 178, p. 477-504.

4 Boiko, T., A. Van Wart, J. H. Caldwell, S. R. Levinson, J. S. Trimmer, and G. Matthews, 2003, Functional specialization of the axon initial segment by isoform-specific sodium channel targeting: J Neurosci, v. 23, p. 2306-13.

5 Caldwell, J. H., K. L. Schaller, R. S. Lasher, E. Peles, and S. R. Levinson, 2000, Sodium channel Na(v)1.6 is localized at nodes of ranvier, dendrites, and synapses: Proc Natl Acad Sci U S A, v. 97, p. 5616-20.

6 Carras, P. L., P. A. Coleman, and R. F. Miller, 1992, Site of action potential initiation in amphibian retinal ganglion cells: J Neurophysiol, v. 67, p. 292-304.

7 Chow, A. Y., V. Y. Chow, K. H. Packo, J. S. Pollack, G. A. Peyman, and R. Schuchard, 2004, The artificial silicon retina microchip for the treatment of vision loss from retinitis pigmentosa: Arch Ophthalmol, v. 122, p. 460-9.

8 Dacey, D. M., B. B. Peterson, F. R. Robinson, and P. D. Gamlin, 2003, Fireworks in the primate retina: in vitro photodynamics reveals diverse LGN-projecting ganglion cell types: Neuron, v. 37, p. 15-27.

9 DeVries, S. H., and D. A. Baylor, 1997, Mosaic arrangement of ganglion cell receptive fields in rabbit retina: Journal of Neurophysiology, v. 78, p. 2048-2060.

10 Fohlmeister, J. F., P. A. Coleman, and R. F. Miller, 1990, Modeling the repetitive firing of retinal ganglion cells: Brain Res, v. 510, p. 343-5.

11 Fohlmeister, J. F., and R. F. Miller, 1997, Mechanisms by which cell geometry controls repetitive impulse firing in retinal ganglion cells: J Neurophysiol, v. 78, p. 1948-64.

12 Fried, S. I., H. A. Hsueh, and F. Werblin, 2007, A method for generating precise temporal patterns of activity with prosthetic stimulation, *in* E. Greenbaum, ed., Artificial Sight: Basic Research, Biomedical Engineering and Clinical Advances, Springer, p. 347-54.

13 Fried, S. I., H. A. Hsueh, and F. S. Werblin, 2006, A method for generating precise temporal patterns of retinal spiking using prosthetic stimulation: J Neurophysiol, v. 95, p. 970-8.
14 Gekeler, F., A. Messias, M. Ottinger, K. U. Bartz-Schmidt, and E. Zrenner, 2006, Phosphenes electrically evoked with DTL electrodes: a study in patients with retinitis pigmentosa, glaucoma, and homonymous visual field loss and normal subjects: Invest Ophthalmol Vis Sci, v. 47, p. 4966-74.
15 Greenberg, R., 1998, Analysis of electrical stimulation of the vertebrate retina - work towards a retinal prosthesis: Dissertation thesis, Johns Hopkins, Baltimore.
16 Greenberg, R. J., T. J. Velte, M. S. Humayun, G. N. Scarlatis, and E. de Juan, Jr., 1999, A computational model of electrical stimulation of the retinal ganglion cell: IEEE Trans Biomed Eng, v. 46, p. 505-14.
17 Gustafsson, B., and E. Jankowska, 1976, Direct and indirect activation of nerve cells by electrical pulses applied extracellularly: J Physiol, v. 258, p. 33-61.
18 Hornig, R., T. Laube, P. Walter, M. Velikay-Parel, N. Bornfeld, M. Feucht, H. Akguel, G. Rossler, N. Alteheld, D. Lutke Notarp, J. Wyatt, and G. Richard, 2005, A method and technical equipment for an acute human trial to evaluate retinal implant technology: J Neural Eng, v. 2, p. S129-34.
19 Humayun, M. S., E. de Juan, Jr., G. Dagnelie, R. J. Greenberg, R. H. Propst, and D. H. Phillips, 1996, Visual perception elicited by electrical stimulation of retina in blind humans: Arch Ophthalmol, v. 114, p. 40-6.
20 Humayun, M. S., E. de Juan, Jr., J. D. Weiland, G. Dagnelie, S. Katona, R. Greenberg, and S. Suzuki, 1999, Pattern electrical stimulation of the human retina: Vision Res, v. 39, p. 2569-76.
21 Humayun, M. S., J. D. Weiland, G. Y. Fujii, R. Greenberg, R. Williamson, J. Little, B. Mech, V. Cimmarusti, G. Van Boemel, G. Dagnelie, and E. de Juan, 2003, Visual perception in a blind subject with a chronic microelectronic retinal prosthesis: Vision Res, v. 43, p. 2573-81.
22 Jenkins, S. M., and V. Bennett, 2001, Ankyrin-G coordinates assembly of the spectrin-based membrane skeleton, voltage-gated sodium channels, and L1 CAMs at Purkinje neuron initial segments: J Cell Biol, v. 155, p. 739-46.
23 Jensen, R. J., J. F. Rizzo, 3rd, O. R. Ziv, A. Grumet, and J. Wyatt, 2003, Thresholds for activation of rabbit retinal ganglion cells with an ultrafine, extracellular microelectrode: Invest Ophthalmol Vis Sci, v. 44, p. 3533-43.
24 Jensen, R. J., O. R. Ziv, and J. F. Rizzo, 2005, Responses of rabbit retinal ganglion cells to electrical stimulation with an epiretinal electrode: J Neural Eng, v. 2, p. S16-21.
25 Koizumi, A., G. Zeck, Y. Ben, R. H. Masland, and T. C. Jakobs, 2007, Organotypic culture of physiologically functional adult mammalian retinas: PLoS ONE, v. 2, p. e221.
26 Kordeli, E., S. Lambert, and V. Bennett, 1995, AnkyrinG. A new ankyrin gene with neural-specific isoforms localized at the axonal initial segment and node of Ranvier: J Biol Chem, v. 270, p. 2352-9.

27 Li, C. L., and A. Bak, 1976, Excitability characteristics of the A- and C-fibers in a peripheral nerve: Exp Neurol, v. 50, p. 67-79.
28 Lo, D. C., A. K. McAllister, and L. C. Katz, 1994, Neuronal transfection in brain slices using particle-mediated gene transfer: Neuron, v. 13, p. 1263-8.
29 Nowak, L. G., and J. Bullier, 1998, Axons, but not cell bodies, are activated by electrical stimulation in cortical gray matter. I. Evidence from chronaxie measurements: Exp Brain Res, v. 118, p. 477-88.
30 Nowak, L. G., and J. Bullier, 1998, Axons, but not cell bodies, are activated by electrical stimulation in cortical gray matter. II. Evidence from selective inactivation of cell bodies and axon initial segments: Exp Brain Res, v. 118, p. 489-500.
31 O'Brien, B. J., T. Isayama, R. Richardson, and D. M. Berson, 2002, Intrinsic physiological properties of cat retinal ganglion cells: J Physiol, v. 538, p. 787-802.
32 Oesch, N., T. Euler, and W. R. Taylor, 2005, Direction-selective dendritic action potentials in rabbit retina: Neuron, v. 47, p. 739-50.
33 Ranck, J. B., Jr., 1975, Which elements are excited in electrical stimulation of mammalian central nervous system: a review: Brain Res, v. 98, p. 417-40.
34 Rasband, M. N., E. Peles, J. S. Trimmer, S. R. Levinson, S. E. Lux, and P. Shrager, 1999, Dependence of nodal sodium channel clustering on paranodal axoglial contact in the developing CNS: J Neurosci, v. 19, p. 7516-28.
35 Rattay, F., 1999, The basic mechanism for the electrical stimulation of the nervous system: Neuroscience, v. 89, p. 335-46.
36 Resatz, S., and F. Rattay, 2004, A Model for the Electrically Stimulated Retina: Mathematical and Computer Modeling of Dynamical Systems, v. 10, p. 93-106.
37 Rizzo, J. F., 3rd, J. Wyatt, J. Loewenstein, S. Kelly, and D. Shire, 2003, Methods and perceptual thresholds for short-term electrical stimulation of human retina with microelectrode arrays: Invest Ophthalmol Vis Sci, v. 44, p. 5355-61.
38 Rizzo, J. F., 3rd, J. Wyatt, J. Loewenstein, S. Kelly, and D. Shire, 2003, Perceptual efficacy of electrical stimulation of human retina with a microelectrode array during short-term surgical trials: Invest Ophthalmol Vis Sci, v. 44, p. 5362-9.
39 Rockhill, R. L., F. J. Daly, M. A. MacNeil, S. P. Brown, and R. H. Masland, 2002, The diversity of ganglion cells in a mammalian retina: J Neurosci, v. 22, p. 3831-43.
40 Roska, B., and F. Werblin, 2001, Vertical interactions across ten parallel, stacked representations in the mammalian retina: Nature, v. 410, p. 583-587.
41 Schiefer, M. A., and W. M. Grill, 2006, Sites of neuronal excitation by epiretinal electrical stimulation: IEEE Trans Neural Syst Rehabil Eng, v. 14, p. 5-13.
42 Sekirnjak, C., P. Hottowy, A. Sher, W. Dabrowski, A. M. Litke, and E. J. Chichilnisky, 2006, Electrical stimulation of mammalian retinal ganglion cells with multielectrode arrays: J Neurophysiol, v. 95, p. 3311-27.
43 Sekirnjak, C., P. Hottowy, A. Sher, W. Dabrowski, A. M. Litke, and E. J. Chichilnisky, 2008, High-resolution electrical stimulation of primate retina for epiretinal implant design: J Neurosci, v. 28, p. 4446-56.

44 Swadlow, H. A., 1992, Monitoring the excitability of neocortical efferent neurons to direct activation by extracellular current pulses: J Neurophysiol, v. 68, p. 605-19.
45 Van Wart, A., J. S. Trimmer, and G. Matthews, 2007, Polarized distribution of ion channels within microdomains of the axon initial segment: J Comp Neurol, v. 500, p. 339-52.
46 Velte, T. J., and R. H. Masland, 1999, Action potentials in the dendrites of retinal ganglion cells: J Neurophysiol, v. 81, p. 1412-7.
47 Wassle, H., 2004, Parallel processing in the mammalian retina: Nat Rev Neurosci, v. 5, p. 747-57.
48 West, D. C., and J. H. Wolstencroft, 1983, Strength-duration characteristics of myelinated and non-myelinated bulbospinal axons in the cat spinal cord: J Physiol, v. 337, p. 37-50.
49 Wollner, D. A., and W. A. Catterall, 1986, Localization of sodium channels in axon hillocks and initial segments of retinal ganglion cells: Proc Natl Acad Sci U S A, v. 83, p. 8424-8.
50 Zrenner, E., D. Besch, K. U. Bartz-Schmidt, F. Gekeler, and V. P. Gabel, 2006, Subretinal chronic multielectrode arrays implanted in blind patients: Invest Ophthalmol Vis Sci, v. 47.

Figure legends

Figure 1: Determining threshold at a single location. (a) Ganglion cell voltage-clamp responses to cathodic stimulus pulses. (a_1) Responses to a 16 μA pulse (three repetitions): the sharp rise and fall of the stimulus artifact are clearly visible (arrows). (a_2) Responses to three 18 μA pulses: an action potential (arrow) is elicited by one of the three pulses. ($a_{3,4}$) Responses to 20 μA and 22 μA pulses: action potentials (arrows) are elicited by 2 and 3 of the pulses respectively. (**b**) Number of elicited spikes is plotted as a function of stimulus pulse amplitude level ('X'). Threshold is defined as the amplitude level at which 2 of 3 pulses elicit spiking. A sigmoid function (dashed line) was fit to the measured points (see next panel). (**c**) Similar to (b), the number of elicited spikes is plotted as a function of pulse amplitude for a different stimulating electrode location. In this case, the amplitude level at which 2 of 3 pulses elicits spiking is ambiguous. Instead, the sigmoid function was used to assign a value of threshold - solid lines intersect the sigmoid curve to determine the threshold level. Scale bar in panel a_1: 100 pA vertical and 1 ms horizontal applies to $a_{2\text{-}4}$.

Figure 2: Threshold maps reveal regions of high and low sensitivity. (**a**) Threshold map for a DS ganglion cell. Each square represents a threshold measurement for that location of the stimulating electrode; the color represents threshold level (colorbar at top). The circle indicates the approximate location of the soma. The thresholds for the locations indicated by 'b' and 'c' were determined in Figures 1 b and 1c respectively. (**b**) The same data from (a) is re-plotted with single colors representing a wider range of threshold amplitudes (scale at bottom). Similar to (a), the circle indicates the approximate location of the soma. As indicated in (a), threshold level increases as the stimulating electrode moved away from the central low threshold region; the blue colors in the periphery of (b) are an artifact of the contour plotting program. Scale bar for panels (a), (b): 100 μm.

Figure 3: Dense sodium-channel staining is limited to a small region of the axon. (**a**) Confocal image stack of a DS ganglion cell. The characteristic morphological features include a relatively large soma as well as bi-stratified and recursive dendritic processes. (**b**) Higher magnification view of the soma and initial portion of the axon. (**c**) Immuno-chemical staining for Ankyrin G (red) reveals several long, thin segments (arrows). The small, punctuate staining is an artifact associated with non-specific binding of one of the antibodies. (**d**) Overlay of (b) and (c) reveals that one of the long Ankyrin G segments is co-extensive with a portion of the axon. Vertical lines from (c) help clarify the edges of the Ankyrin G staining. (**e-h**) Similar to (a-d) except Pan Sodium Antibody used in place of Ankyrin G. Scale bar in (a): 25 μm applies to (e). Scale bar in (b): 25 μm applies to (c) and (d); scale bar in (f): 25 μm applies to (g) and (h).

Figure 4: Length and location of high-density sodium-channel regions in DS cells are variable. The length of the region (inset, distance between 1 and 2) was plotted vs. the distance between the soma and the proximal edge of the region (inset, distance between 2 and 3). Each point is from a different cell. The circled point is from the cell shown in the inset. Inset scale bar: 25 μm.

Figure 5: Dense sodium-channel region is co-localized to the region where the axon diameter decreases. *Bottom*: View of the soma and axon from a DS ganglion cell (green) and Pan immunostaining (red). The vertical lines indicate the approximate extent of the dense sodium-channel region. *Top*: The same DS cell from the bottom panel. The vertical lines reveal that the dense sodium-channel region is in a portion of the axon where the diameter transitions from large to small (compare the axon diameter at the right and left lines). Scale bar: 20 μm.

Figure 6: High density sodium-channel and low threshold regions are spatially co-extensive. The thick vertical line on the right indicates the edge of the soma. Each thin red line corresponds to a region of high density sodium channels: the length of the line is proportional to the length of the high-density region; the distance between the line and the 'soma' line is proportional to the distance between the high-density region and the soma. The thick red line represents the mean (size and location) of all high-density regions. Similarly, each thin blue line corresponds to the length and

position of each region of low threshold. The thick blue line represents the mean size and location of all regions of low threshold. The dotted red and blue lines correspond to the high-density region and low threshold region (respectively) from the one cell in which both measurements were taken. The thin vertical line represents a distance of 5 μm from the soma; the region between the two lines is where most axon bends were found. Scale bar: 20 μm.

Figure 7: Ankyrin G staining is co-extensive with the region of low threshold. (**a**) Threshold map of a DS ganglion cell. The map has been rotated ~20° in order to align it to the Ankyrin G image in (c) - see Methods. The threshold values given by each color are identical to those in Figure 2a. (**b**) Overlay of the threshold map with the Ankyrin G staining. The soma ('s') and axon (arrow) are clearly visible. The white vertical lines extend up from (c) and are used to clarify the region of high density Ankyrin G staining. (**c**) Ankyrin G staining in the same cell as (a). Scale bar in (a): 25 μm (applies to all panels).

Figure 8: Axon bend of DS ganglion cells. (**a**) Cross-sectional view of a typical DS ganglion cell (green); the axon emerges from the vitreal (top) half of the soma and immediately 'bends' (arrow) to run along the NFL (top of figure). Portions of axons from other ganglion cells are also visible (arrowhead). (**b**) Cross sectional view of an atypical DS axon - the axon 'bends' down (toward the scleral side of the retina, arrow) and runs horizontally for >100 μm. (**c**) Cross sectional view of a typical (DS) axon bend with subsequent axonal oscillation: after reaching NFL the axon descends and re-ascends. (**d-f**). Cross-sectional view (d), whole mount view (f) and an oblique view (e) of the ganglion cell from (c). Pan sodium staining (red) reveals a band of axon fibers ('BAF') coursing along the NFL. The single axon fiber (green) descends to pass under the band of axon fibers and then re-ascends back to the NFL. The oblique view is approximately mid-way between the cross sectional and top views. (**g**) Cross-sectional view of the axon from the one DS cell for which both threshold map and immunochemistry were obtained. Similar to (b), the axon runs horizontally before curving up to run along the NFL. The region of low threshold (blue bar) occurs along this flat portion of the axon. Threshold values rise sharply (Fig. 7) as the axon rises up towards the NFL (*). Scale bar in (a): 25 μm, applies to (b); scale bar in (c): 25 μm applies to (d)-(f), scale bar in (g): 25 μm.

Figure 9: Low thresholds are found in segments of the distal axon. The inset shows a threshold map that extends out along the distal axon, approximately 1.1 mm from the soma. The gaps arise from incomplete sampling along the distal axon. Similar to Figure 2, each pixel of the threshold map contains an individual threshold measurement; the reduced scale makes it difficult to resolve individual pixels. The colorbar scale is identical to Figure 2a. Threshold at each location along the axon (dashed line) is plotted as a function of distance from the soma. The circled point indicates the threshold level when the electrode was over the soma. Scale bar inset, 100 μm.

Figure 10: Variability in axon properties across different ganglion cell sub-types. (**a**) Threshold maps for a Local Edge Detector (LED, left) and a DS ganglion cell (right) plotted at the same scale. The black circles indicate the position of the soma. The colorbar scale is identical to Figure 2. (**b**) Left: A non-DS ganglion cell soma and axon (green) with immunostaining for sodium-channels (Ankyrin G, red); the white bar indicates the approximate extent of the region of high-density sodium-channels. Middle/Left panels: Similar images for 2 other non-DS cells. (**c**) Two adjacent ganglion cells (green) extend dendritic processes down into the inner plexiform layer and axons up to the nerve fiber layer (arrowhead). For the cell on the right, the axon emerges from the approximate midline of the soma (arrow) and ascends slowly to the NFL while the axon of the left cell emerges from the vitreal end of the soma (arrow) and ascends directly to the NFL. The nerve fiber layer (top, red) is visible as a result of immuno-staining for Pan. Scale bar: (a), 100 μm; (β), 25 μm; in (c), 20 μm.

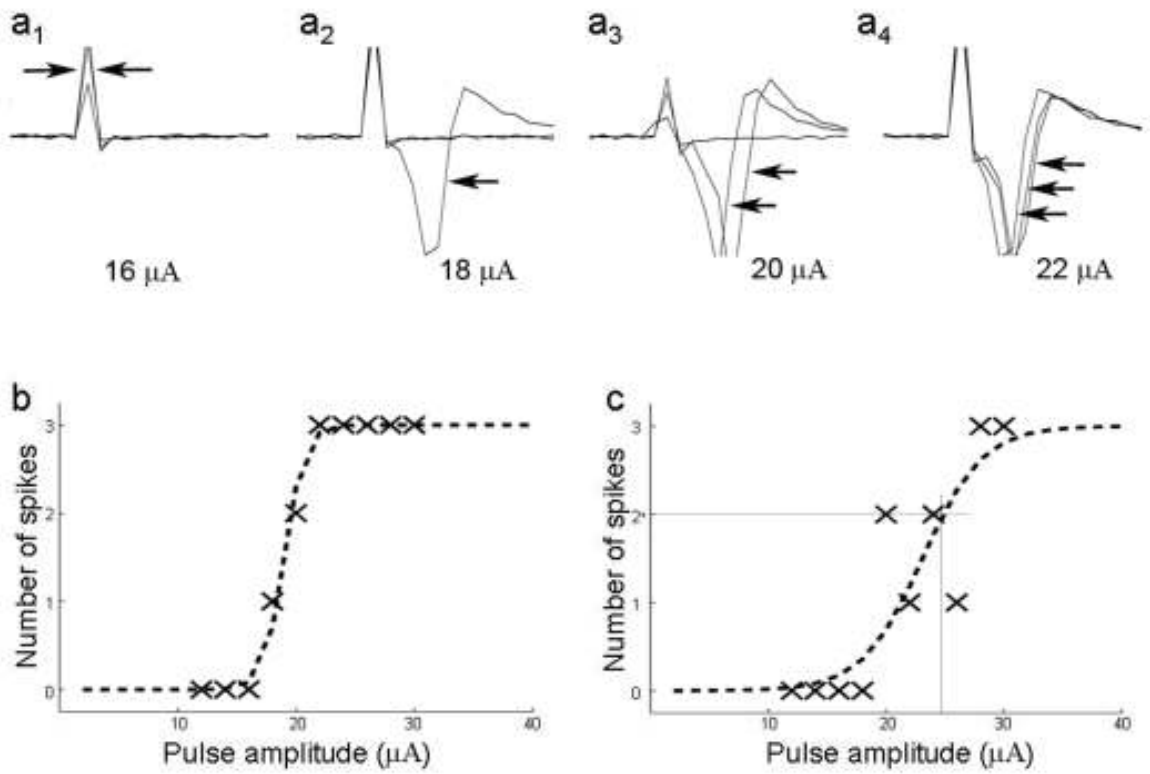
a1
a2
a3
a4
16 μA
18 μA
20 μA
22 μA
b
c
Number of spikes
Pulse amplitude (μA)
0
1
2
3
10
20
30
40

Figure 1

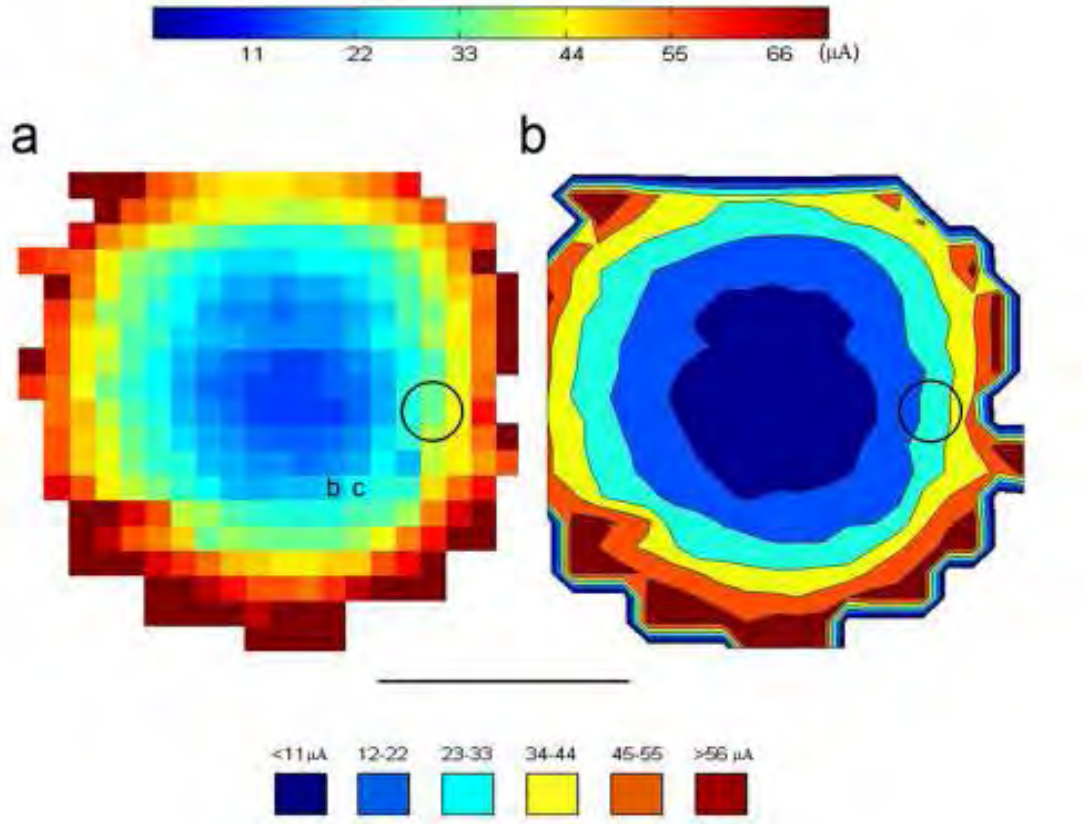

Figure 2

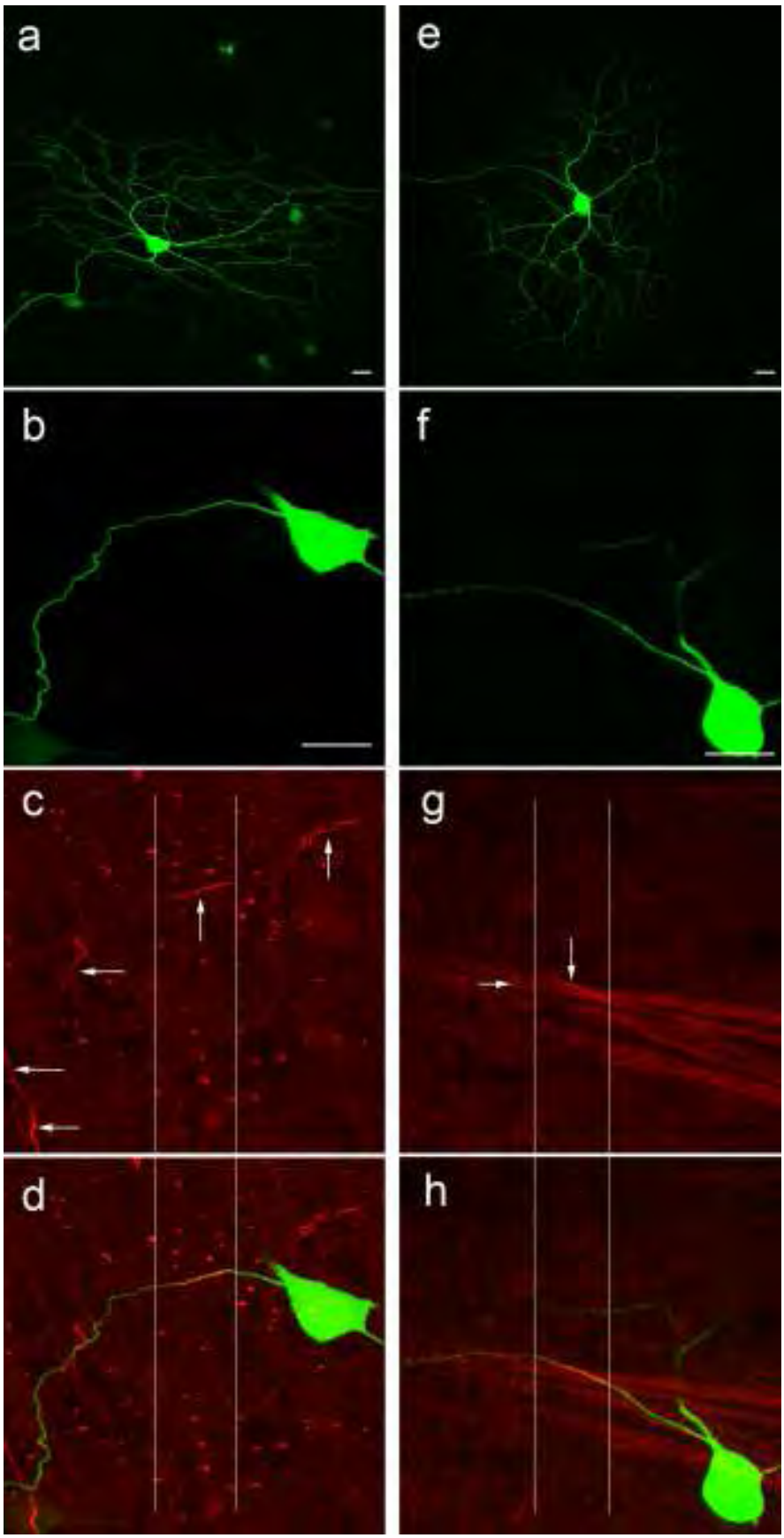
a
e
b
f
c
g
d
h

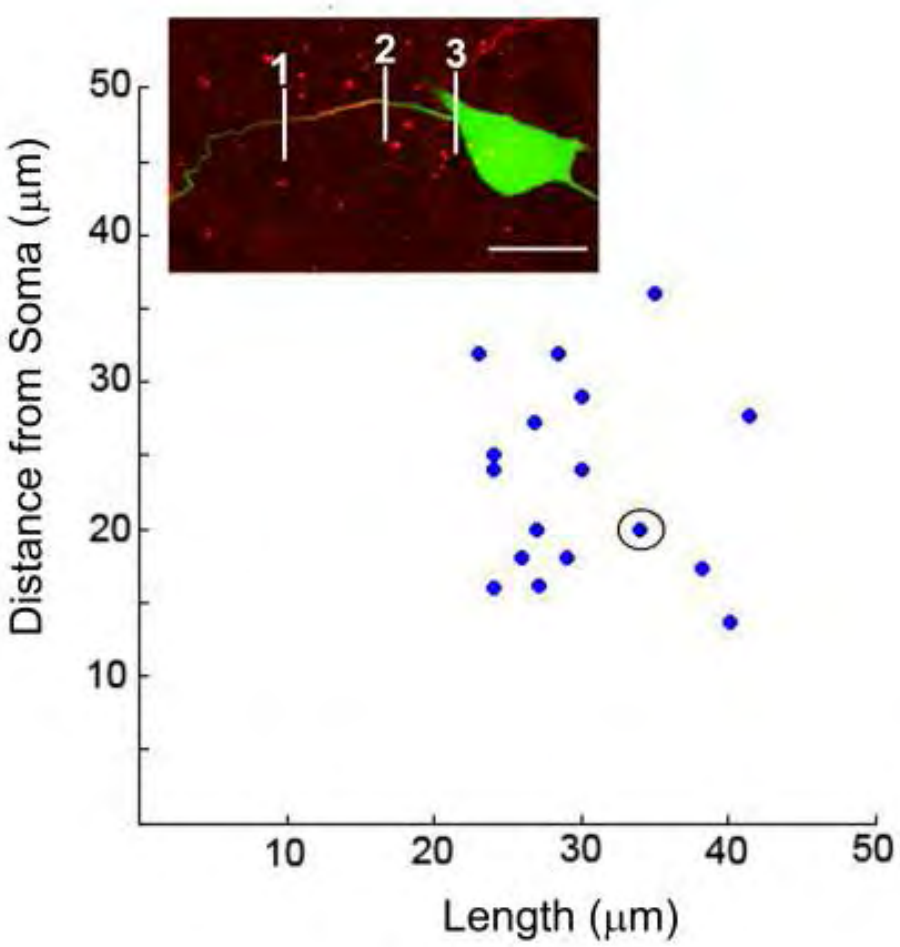

Figure 4

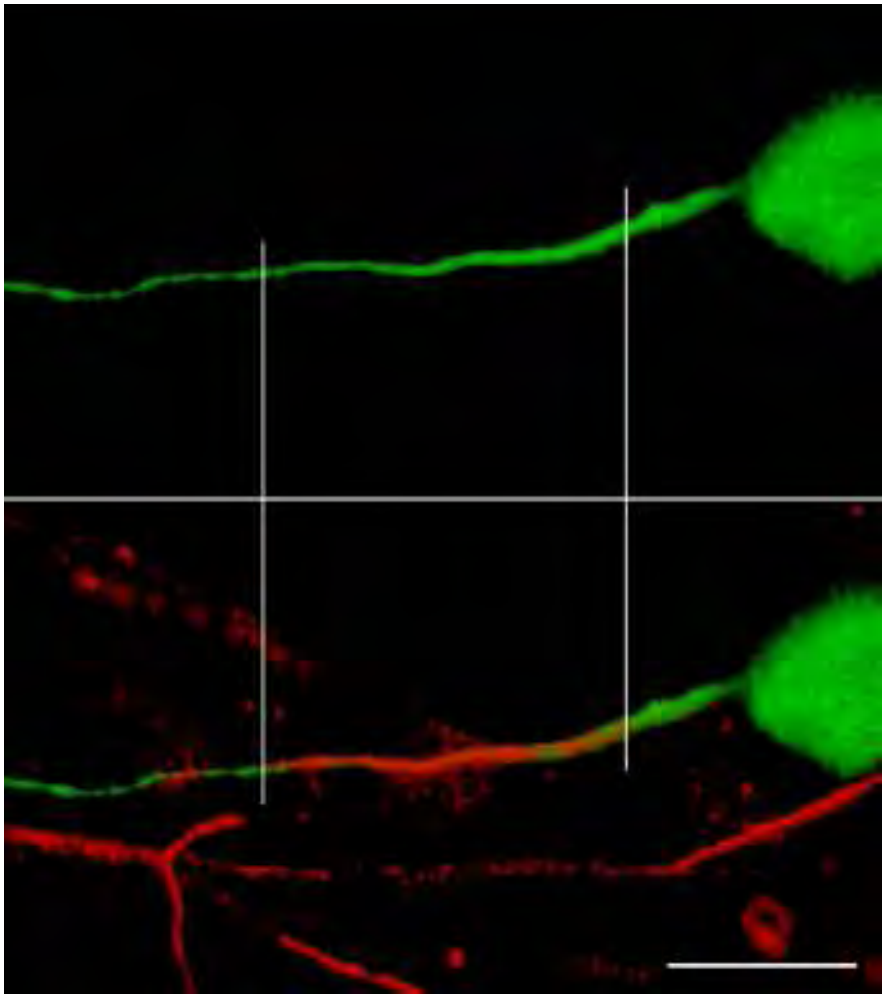

Figure 5

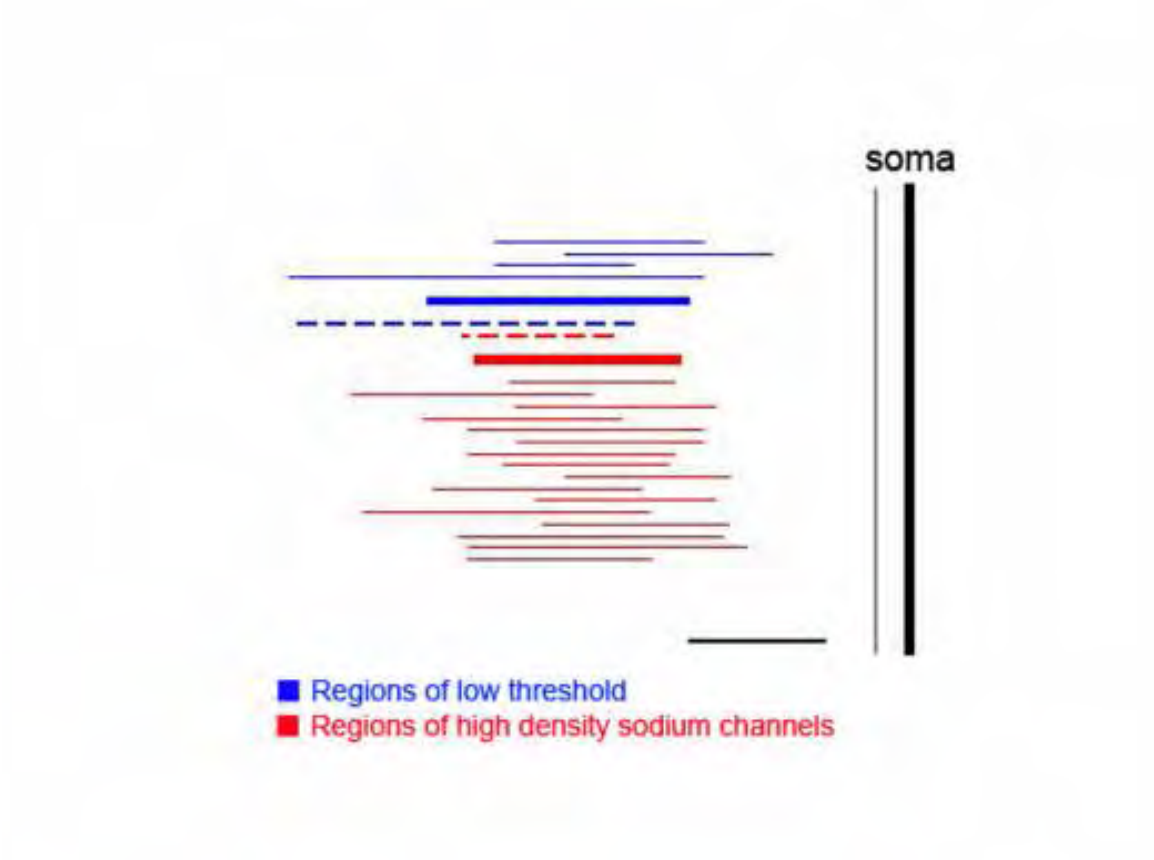
soma
Regions of low threshold
Regions of high density sodium channels

Figure 6

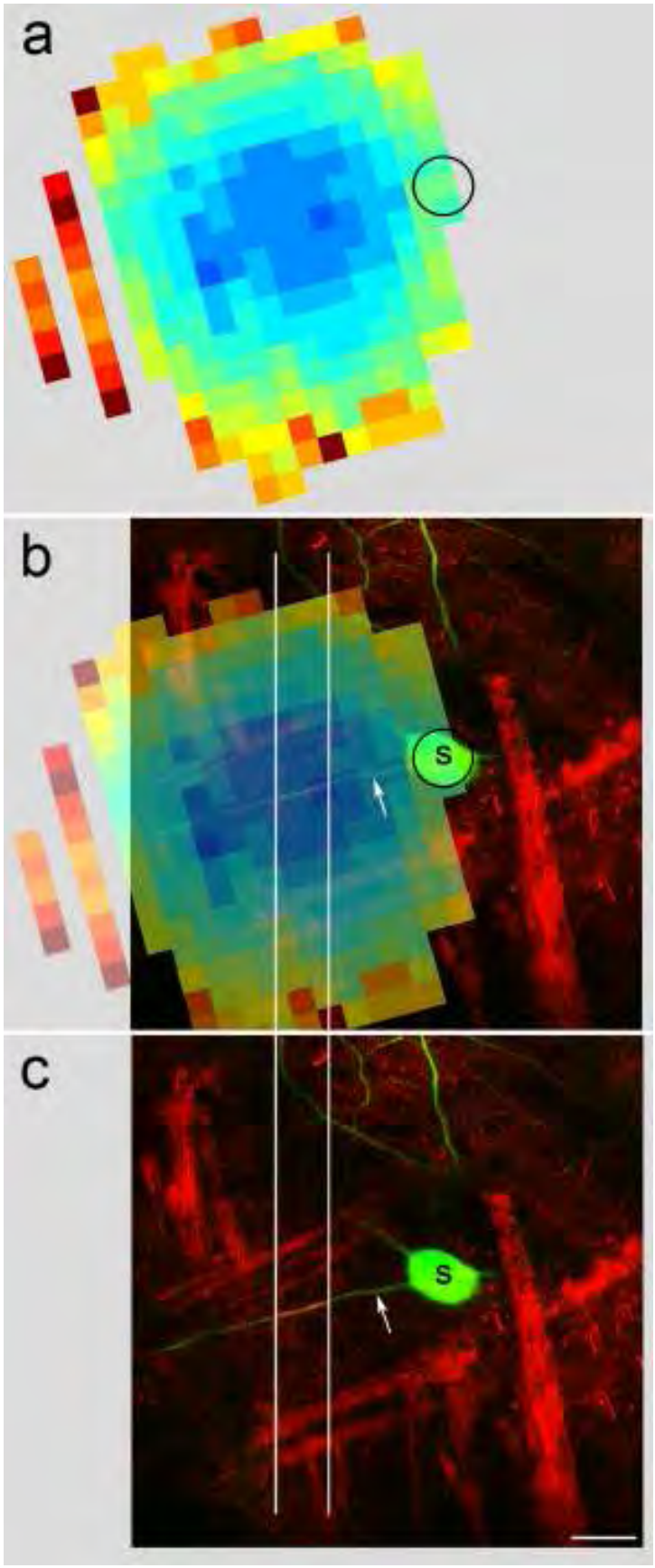
a
b
s
c
s

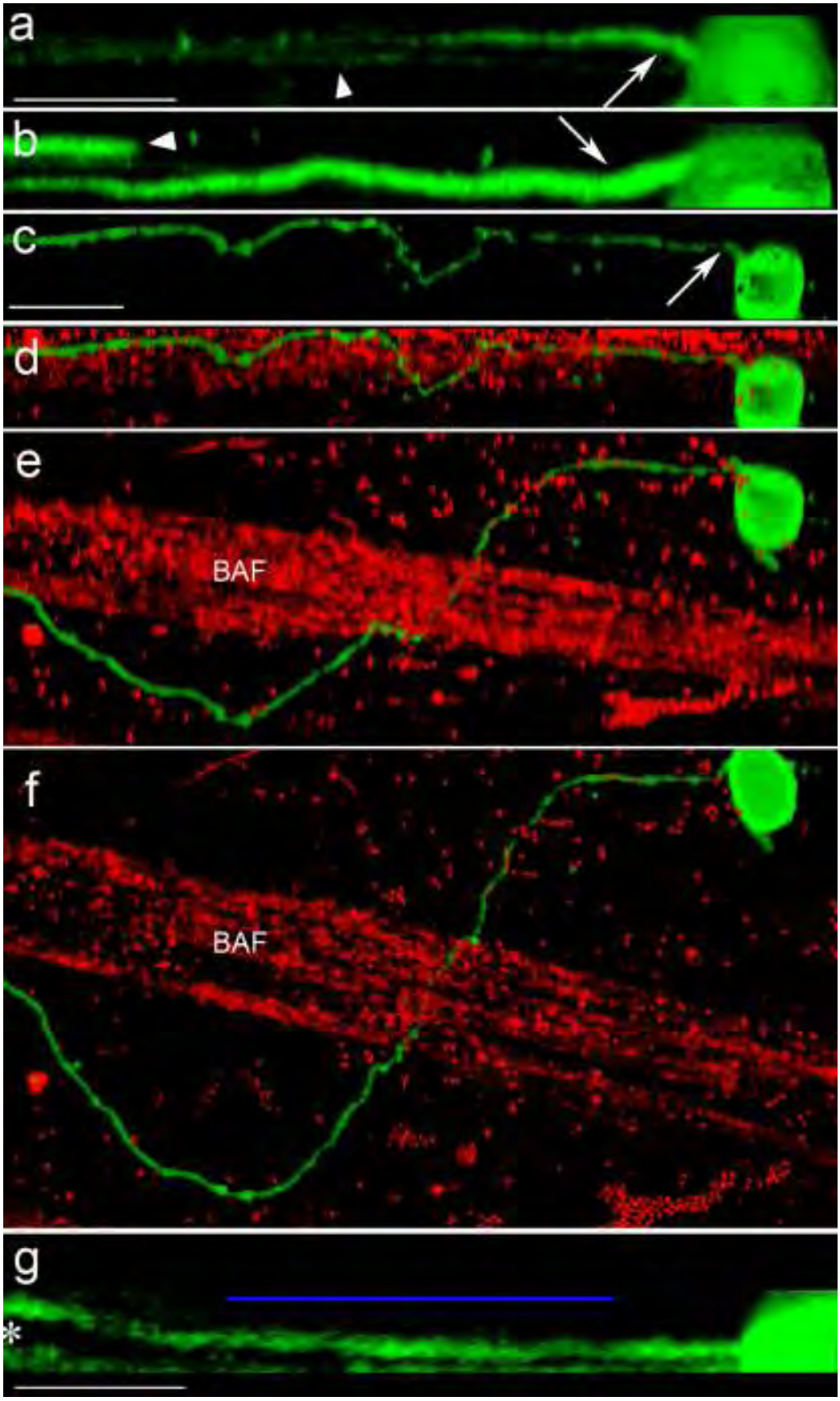
a
b
c
d
e
BAF
f
BAF
g
*

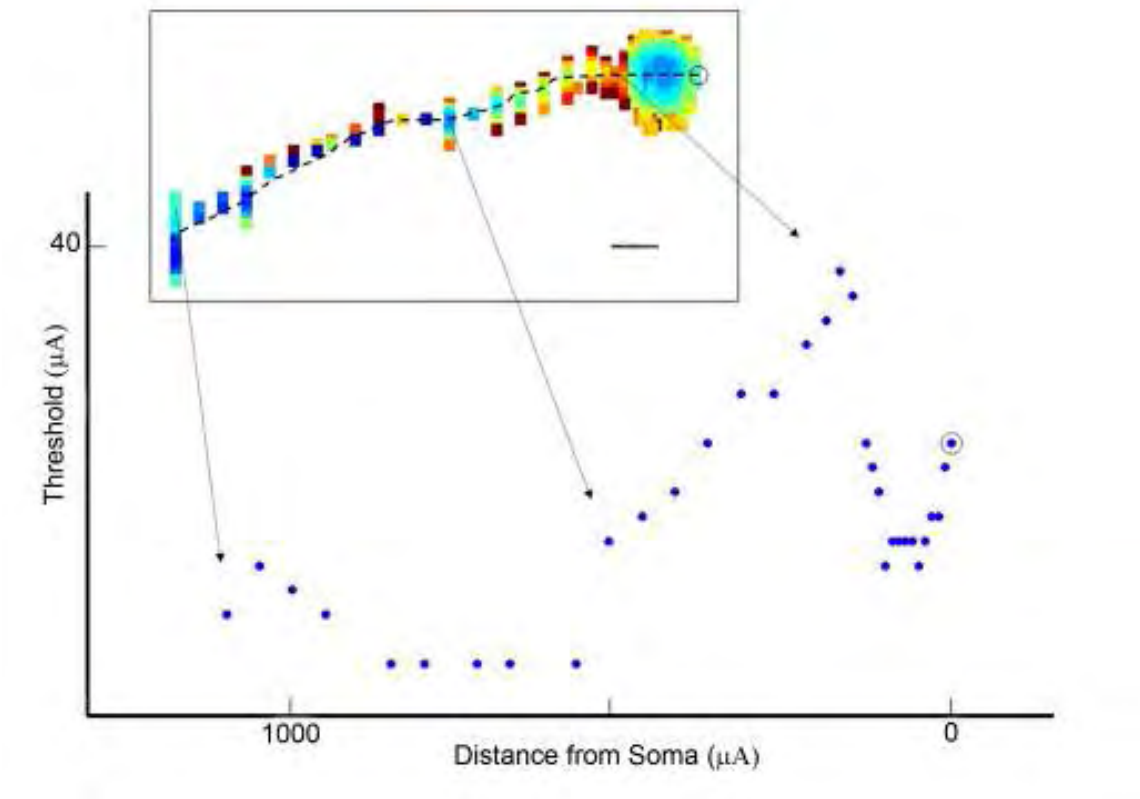

Figure 9

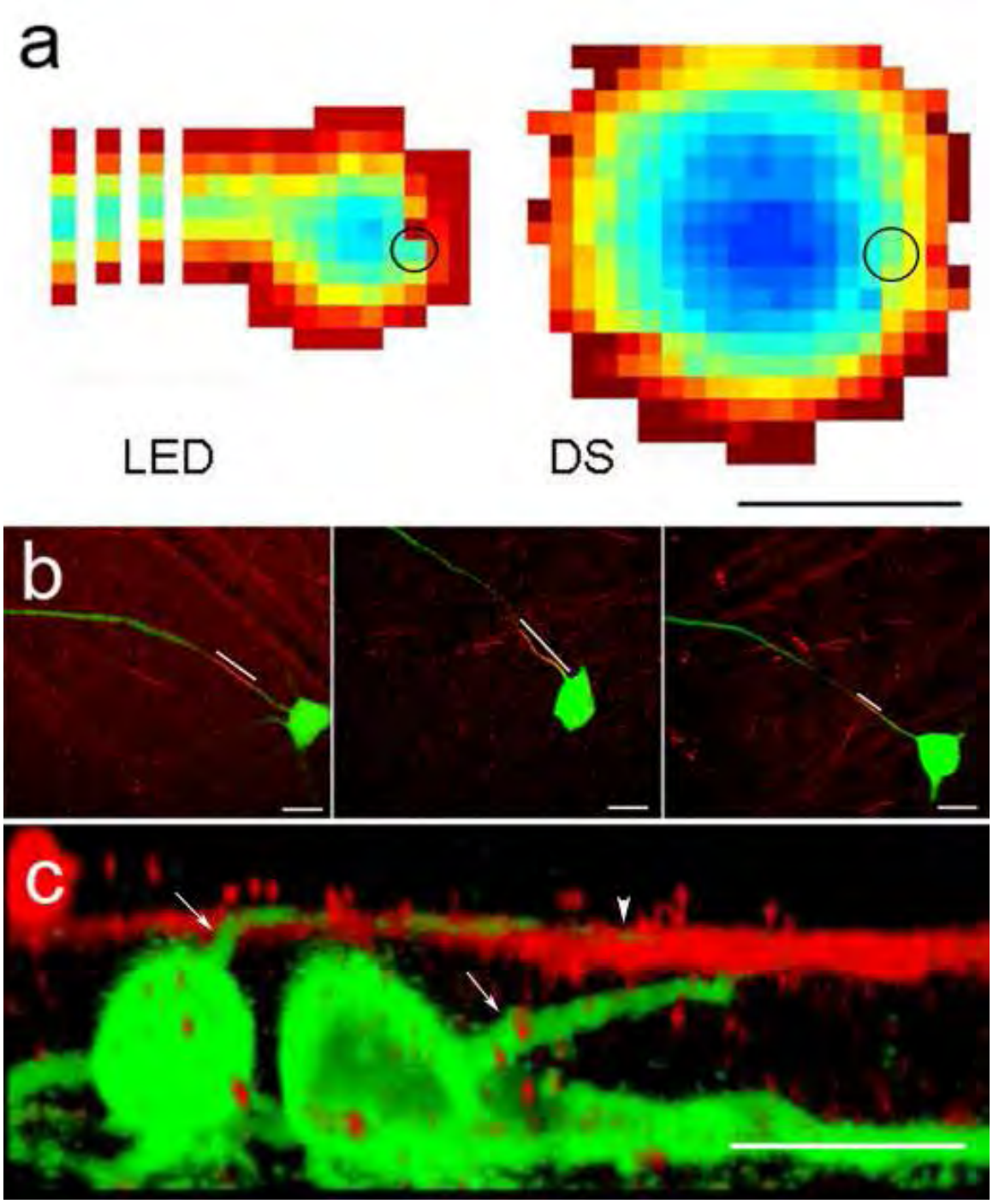

Figure 10